THESIS FOR THE DEGREE OF DOCTOR OF PHILOSOPHY

Assessment and improvements of thermal-hydraulic correlations and methods for the analysis of the Jules Horowitz Reactor

ALBERTO GHIONE

Division of Subatomic and Plasma Physics
Department of Physics
Chalmers University of Technology
SE-412 96 Göteborg, Sweden, 2017

Assessment and improvements of thermal-hydraulic correlations and methods for the analysis of the Jules Horowitz Reactor
ALBERTO GHIONE
ISBN 978-91-7597-520-7

Doktorsavhandling vid Chalmers Tekniska Högskola
Ny serie nr 4201
ISSN 0346-718X
CTH-NT-325

Division of Subatomic and Plasma Physics
Department of Physics
Chalmers University of Technology
SE-412 96 Göteborg
Sweden

Cover: Single-phase turbulent heat transfer coefficient in a JHR fuel assembly.

Chalmers Reproservice
Göteborg, Sweden 2017

Assessment and improvements of thermal-hydraulic correlations and methods for the analysis of the Jules Horowitz Reactor

ALBERTO GHIONE
Division of Subatomic and Plasma Physics, Department of Physics
Chalmers University of Technology

ABSTRACT

Nuclear research reactors are used to test materials for current and future nuclear technologies, and to produce radioisotopes for medical purposes. Most of the existing Material Testing Reactors in Europe have operated for more than 50 years and new ones are needed. Therefore the Jules Horowitz Reactor (JHR) is under construction at the French Alternative Energies and Atomic Energy Commission (CEA), on the Cadarache site.

The JHR will allow irradiation experiments with high neutron fluxes, at fast and thermal energies. In order to cope with the considerable heat fluxes generated during operations, the core configuration consists of fuel assemblies with parallel narrow channels, where coolant flows at high velocity. Such a design is unique and specific simulation capabilities have to be developed for the analysis.

This doctoral research investigates possible improvements of the thermal-hydraulic modeling of the JHR, and is arranged in three parts. In the first part, correlations for the single-phase turbulent friction and heat transfer, for the fully developed boiling heat transfer, and for the critical heat flux, respectively, are assessed and their accuracy is quantified, against the SULTAN-JHR experiments. These experiments were carried out in heated narrow channels comparable to the JHR ones. It is shown that the single-phase turbulent correlations valid for standard nuclear systems, can perform poorly when applied to the typical conditions of the JHR. Thus, new best-fitting relationships are derived. For fully developed boiling in narrow channels, the Forster-Greif correlation can be considered a reliable option. As regards the modeling of the critical heat flux, the Sudo correlation can provide satisfactory predictions. These results are then used to modify the thermal-hydraulic system code CATHARE for the purpose of a more realistic analysis of the JHR.

The second part is focused on the onset of flow instability, which is a primary concern in systems with parallel channels as the JHR, since it can lead to undesirable boiling crisis. In view of this, several criteria are evaluated with experiments in narrow channels from both the SULTAN-JHR program and the literature. Conservative predictions can be obtained with Saha-Zuber KIT correlation. Furthermore, some criteria are optimized with respect to the available experimental data for narrow channels.

In the third part, the analysis of a postulated accident in the JHR, namely a station black-out, is performed with a best-estimate plus uncertainty approach, combined with the CATHARE code as modified in the first part of the thesis. As a result, the impact of different input and modeling uncertainties on the simulation is estimated, and the most influential uncertain parameters are identified.

Keywords: Jules Horowitz Reactor; Material Testing Reactor; Narrow channels; Thermal-hydraulic correlations; Heat transfer; Critical heat flux; Flow instability; Safety analysis; Best-Estimate; Uncertainty

List of Publications

This thesis is an introduction to and a summary of the work published in the following papers:

PAPER I

A. Ghione, B. Noel, P. Vinai and C. Demazière. "Assessment of thermal-hydraulic correlations for narrow rectangular channels with high heat flux and coolant velocity"
International Journal of Heat and Mass Transfer, 99:344-356, 2016
The first author carried out the survey of existing correlations, simulated the experiments, analyzed the results, and wrote the manuscript.

PAPER II

A. Ghione, B. Noel, P. Vinai and C. Demazière. "Assessment of Critical Heat Flux correlations in narrow rectangular channels"
Proceedings of the 11th International Topical Meeting on Nuclear Thermal Hydraulics, Operation and Safety (NUTHOS-11), Gyeongju, Korea, Oct. 9-13 2016 (*Peer-reviewed*)
The first author carried out the survey of existing correlations, simulated the experiments, analyzed the results, and wrote the manuscript.

PAPER III

A. Ghione, B. Noel, P. Vinai and C. Demazière. "Criteria for onset of flow instability in heated vertical narrow rectangular channels at low pressure: an assessment study"
International Journal of Heat and Mass Transfer, 105:464-478, 2017
The first author carried out the survey of existing criteria, collected the experiments from the literature, simulated the experiments, analyzed the results, and wrote the manuscript.

PAPER IV

A. Ghione, B. Noel, P. Vinai and C. Demazière. "Uncertainty and sensitivity analysis for the simulation of a station blackout scenario in the Jules Horowitz Reactor"
submitted to Annals of Nuclear Energy
The first author performed the simulations, analyzed the results, and wrote the manuscript.

Other publications related to the work:

A. Ghione, B. Noel, P. Vinai and C. Demazière. "On the prediction of single-phase forced convection heat transfer in narrow rectangular channels"
Proceedings of the 10th International Topical Meeting on Nuclear Thermal Hydraulics, Operation and Safety (NUTHOS-10), Okinawa, Japan, Dec. 14-18 2014 (*Peer-reviewed*)

A. Ghione, B. Noel, P. Vinai and C. Demazière. "Wall superheat prediction in narrow rectangular channels under Fully Developed Boiling of water at low pressures"
Proceedings of the 16th International Topical Meeting on Nuclear Reactor Thermal Hydraulics (NURETH-16), Chicago, USA, Aug. 30 - Sep. 4 2015 (*Peer-reviewed*)

A. Ghione. "Improvement of the nuclear safety code CATHARE based on thermal-hydraulic experiments for the Jules Horowitz Reactor"
Licentiate thesis: CTH-NT-306, Chalmers University of Technology, Göteborg, Sweden, 2015.

Contents

Nomenclature

Acronym	Description
$AECL-UO$	Atomic Energy of Canada Ltd. - University of Ottawa
BE	Best-Estimate
$BEPU$	Best-Estimate Plus Uncertainty
$CATHARE$	Code for Analysis of THermalhydraulics during an Accident of Reactor and safety Evaluation
CEA	Commissariat à l'Énergie Atomique et aux énergies alternatives (France)
CHF	Critical Heat Flux
$CIAU$	Code with the capability of Internal Assessment of Uncertainty
$CSAU$	Code Scaling, Applicability and Uncertainty method
DNB	Departure from Nucleate Boiling
dpa	displacements per atom
EdF	Électricité de France
FDB	Fully Developed Boiling
FE	Flow Excursion
FIR	Flow Instability Ratio
GRS	Gesselschaft für Angalen und Reaktorsicherheit (Germany)
$IRSN$	Institut de Radioprotection et de Sûreté Nucléaire (France)
ITF	Integral Test Facility
JHR	Jules Horowitz Reactor
MTR	Material Testing Reactor
NPP	Nuclear Power Plant
NVG	Net Vapor Generation
OFI	Onset of Flow Instability
ONB	Onset of Nucleate Boiling
OSV	Onset of Significant Void
PCT	Peak Cladding Temperature
pdf	probability distribution function
SBO	Station Blackout
SET	Separate Effect Test
SRC	Standardized Regression Coefficient
SRS	Simple Random Sampling

Symbol	Dimensions	Description
		General Symbols
A	m^2	Flow area
AR	-	Aspect ratio $AR = \frac{e_{ch}}{l_{ch}}$
c_p	J/kg/K	Specific heat capacity
D_{heat}	m	Heated diameter $D_{heat} = \frac{4A}{P_{heat}}$
D_{hydr}	m	Hydraulic diameter $D_{hydr} = \frac{4A}{P_{wet}}$
e_{ch}	m	Channel gap
f	-	Friction factor
g	m/s^2	Acceleration of gravity $g = 9.8066$
G	$kg/m^2/s$	Mass flux $G = \dot{m}/A = \rho v$
G^*	-	Dimensionless mass flux $G^* = \frac{G}{\sqrt{\lambda g \rho_g (\rho_l - \rho_g)}}$
Gr	-	Grashof number $Gr = \frac{g\beta\rho^2 D_{hydr}^3}{\mu^2} \lvert T_w - T_l \rvert$
h	$W/m^2/K$	Heat transfer coefficient
i	J/kg	Specific enthalpy
i_{lg}	J/kg	Latent heat of vaporization
Δi_{sub}	°C	Liquid sub-cooling $\Delta i_{sub} = i_{l,sat} - i_l$
Δi^*_{sub}	-	Dimensionless liquid sub-cooling $\Delta i^*_{sub} = \frac{\Delta i_{sub}}{i_{lg}}$
k	W/m/K	Thermal conductivity
l_{ch}	m	Wetted channel width
l_{heat}	m	Equivalent heated width $l_{heat} = \frac{P_{heat}}{2}$
L_{heat}	m	Heated channel length
$\dot{m}$	kg/s	Mass flow-rate
Nu	-	Nusselt number $Nu = \frac{hD_{hydr}}{k}$
p	Pa	Pressure
Δp	Pa	Pressure drop
Pe	-	Peclet number $Pe = RePr$
Pr	-	Prandtl number $Pr = \frac{c_p \mu}{k}$
P_{heat}	m	Heated perimeter
P_{wet}	m	Wetted perimeter
q''	W/m^2	Heat flux in CATHARE
Ra	-	Rayleigh number $Ra = GrPr$
Re	-	Reynolds number $Re = \frac{GD_{hydr}}{\mu}$
St	-	Stanton number $St = \frac{Nu}{RePr} = \frac{\phi}{Gc_{p,l}\Delta T_{sub}}$
S_{heat}	m^2	Heated surface
t	s	Time
T	°C	Temperature
ΔT_{sat}	°C	Wall superheat $\Delta T_{sat} = T_w - T_{sat}$
ΔT_{sub}	°C	Liquid sub-cooling $\Delta T_{sub} = T_{sat} - T_l$
x	-	Steam quality
z	m	Axial distance

Symbol	Dimensions	Description
		Greek Symbols
α	-	Void fraction
β	$1/^{\circ}C$	Volumetric expansion coefficient $\beta = -\frac{1}{\rho}\left(\frac{\partial \rho}{\partial T}\right)_p$
λ	m	Laplace length $\lambda = \frac{\sqrt{\sigma}}{\sqrt{g(\rho_l - \rho_g)}}$
μ	$kg/m/s$	Dynamic viscosity
ρ	kg/m^3	Density
σ	kg/s^2	Surface tension
ϕ	W/m^2	Heat flux
ϕ^*_{CHF}	-	Dimensionless heat flux $\phi^*_{CHF} = \frac{\phi_{CHF}}{i_{lg}\sqrt{\lambda g \rho_g (\rho_l - \rho_g)}}$

	Subscripts
$_{ch}$	channel
$_{CHF}$	Critical Heat Flux
$_{cor}$	corner
$_{g}$	gas (or vapor) phase
$_{heat}$	heated
$_{in}$	channel inlet
$_{l}$	liquid phase
$_{lam}$	laminar
$_{max}$	maximum
$_{nb}$	nucleate boiling
$_{out}$	channel outlet
$_{pl}$	plate
$_{sat}$	saturation
$_{sub}$	subcooled
$_{turb}$	turbulent
$_{w}$	wall

Chapter 1

Introduction

1.1 The Jules Horowitz Reactor

Material Testing Reactors (MTRs) are of strategic importance to support commercial Nuclear Power Plants (NPPs), develop new technologies for future reactors, and produce radioisotopes for medical use. The majority of the existing European MTRs have operated for more than 50 years (see Table 1.1), and they are close to their end of life.

Table 1.1: List of the main MTRs in Europe.

Country	**Reactor name**	**First criticality**	**Power [MWth]**
Czech Rep.	LVR15	1957	10
Norway	Halden	1960	19
Netherlands	HFR	1961	45
Belgium	BR2	1962	100
Poland	Maria	1974	30

In view of this, a new research reactor, namely the Jules Horowitz Reactor (JHR) [1], is under construction at CEA on the Cadarache site, in France. Its first criticality is planned for the year 2022. The project relies on an international cooperation between several industrial and institutional partners.

The main objectives of the JHR are [1]:

- The study of materials and nuclear fuels for the current Light Water Reactors (LWRs). The main focus will be on ageing (radiation damage for in-core experiments up to 16 dpa/y) and corrosion of materials under irradiation, and qualification of innovative fuels.
- The development and qualification of materials and nuclear fuels for future reactors, such as GEN-IV systems.
- The support and development of knowledge and expertise in the field of nuclear engineering.
- The production of radionuclides for medical applications. In particular, the reactor is planned to provide up to 50% of the European demand of Tc-99, which is extensively used in nuclear medicine [2].

The JHR is a 100 MWth pool-type thermal reactor, where light water is used for both cooling and neutron moderation, and the nuclear fuel (for the starting configuration) is U_3Si_2 with an enrichment in uranium-235 lower than 30%. The core has a diameter of 710 mm and an active length of 600 mm. It is placed in a pressurized tank, surrounded by a beryllium reflector, at the bottom of a 10 meters deep reactor pool. The core can host 34 to 37 nuclear fuel assemblies. The design of the fuel assembly is cylindrical and consists of a set of curved plates that are arranged in 8 concentric rings with stiffeners, as displayed in Figure 1.1.

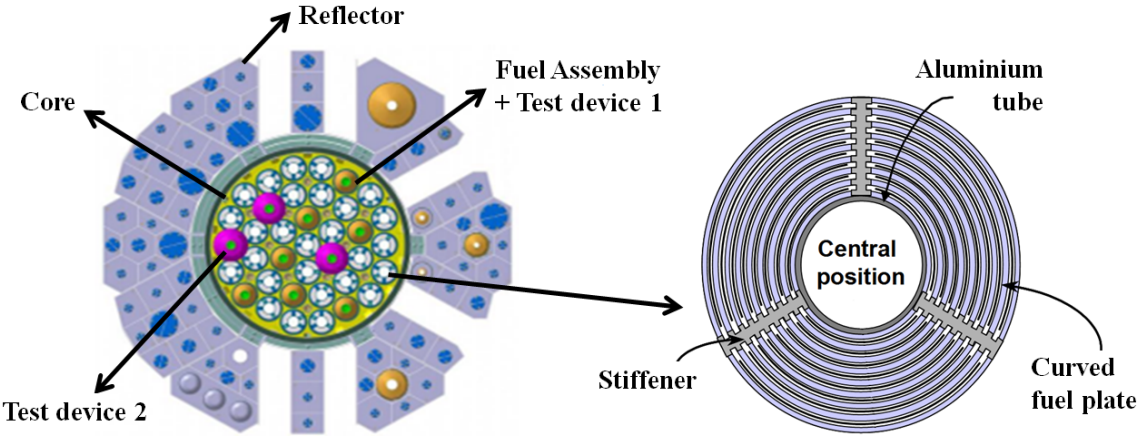

Figure 1.1: Schematic representation of the JHR core and fuel assembly. Courtesy of CEA.

The narrow channels between the fuel plates have an average gap size equal to 1.95 mm. In the central zone of the fuel assembly a control rod can be inserted. The core is cooled by upward forced convection of water. Considering the power and the small core volume, high power density and high heat fluxes can be reached. Therefore, high velocities of the coolant are required to remove efficiently the generated power. The nominal operating conditions are summarized in Table 1.2.

Table 1.2: JHR nominal operating conditions.

Core power [MWth]	100
Power density [kW/l]	460
Maximum heat flux [MW/m^2]	5.5
Maximum coolant velocity [m/s]	15
Core mass flow rate [m^3/h]	7400
Outlet core pressure [MPa]	0.69
Inlet coolant temperature [°C]	30

The arrangement of the reactor allows to load 20 simultaneous experiments. Experimental devices can be introduced in the reflector, in the central zone of a fuel assembly (test device 1 in Figure 1.1), or replace an entire fuel assembly (test device 2). Experiments will be carried out under different irradiation conditions, since high fast and thermal neutron fluxes could be produced in the core and in the reflector, respectively (up to $5 \cdot 10^{14}$ $\frac{neutrons}{cm^2\ s}$).

1.2 Objective of the research work

Due to the unique design and operating conditions of the JHR, specifically tailored simulation capabilities have to be used for reliable analyses of the system behavior. In order to develop these computational capabilities, assessment studies against experimental data or reference solutions play an important role.

The current doctoral research investigates possible advancements of the thermal-hydraulic modeling of the JHR, and consists of three parts.

The first part is related to the assessment of correlations for the thermal-hydraulic system code CATHARE with respect to the JHR features. CATHARE is based on a transient 2-fluid 6-equation model, complemented by proper closure laws for single- and two-phase flows. It has been extensively validated for conditions that are typical of commercial LWRs [3], and it has been mostly used for the safety analysis of these types of reactors. In order to extend its range of applicability to the JHR case, additional validation work is required. Therefore, the correlations implemented in CATHARE and other alternative correlations available from the literature, are evaluated with proper experiments, so that their accuracy can be quantified and the most advantageous options can be determined. The experiments were carried out in the SULTAN-JHR facility at CEA-Grenoble, using narrow rectangular channels and conditions that are representative of the JHR core.

The second part concerns criteria for predicting the Onset of Flow Instability (OFI). The onset of flow instability is a limiting safety phenomenon in nuclear reactors as the JHR, where the core cooling channels are arranged in a parallel configuration and the coolant is in sub-cooled conditions. In fact, the phenomenon may arise from uneven distributions of power and flow over the core, and eventually lead to flow starvation and boiling crisis in some of the channels. In view of this, several criteria are tested against a large database of OFI experiments in narrow rectangular channels; then the most appealing ones are optimized for the JHR.

The objective of the last part of the work is to provide a thermal-hydraulic framework for the safety analysis of the JHR, where the degree of conservatism can be reduced and a more realistic estimation of the reactor safety parameters can be obtained. For this purpose, the CATHARE code modified according to the outcomes from the first part, is combined with a Best-Estimate Plus Uncertainty (BEPU) methodology. The approach is applied to analyze a hypothetical Station Blackout (SBO) scenario in the JHR, and to propagate relevant uncertainties associated with the inputs and the physical models, to the code results. In addition, the most influential input uncertainties are identified through a sensitivity analysis.

1.3 Outline of the thesis

This thesis is arranged in 7 chapters. In Chapter 2, a description of the thermal-hydraulic phenomena that are relevant to the work, is given. The first part of the thesis is presented in Chapter 3 and it is related to Paper I and Paper II. In particular, the CATHARE code is introduced; the SULTAN-JHR experiments used for evaluating the thermal-hydraulic correlations, are described; the results of the assessment are discussed, together with the possible improvements of CATHARE for the JHR case. The focus is on correlations for single-phase friction, single-phase turbulent

heat transfer, fully developed boiling, critical heat flux, and the model for the transition from laminar to turbulent flow. The second part of the work is discussed in Chapter 4 and it is a summary of Paper III. Accordingly, the flow excursion experiments in narrow channels and the main outcomes from the study of different OFI criteria are presented. The third part of the thesis consists of Chapter 5 and 6. In Chapter 5, the background of Paper IV is provided and includes two parts: first, nuclear reactor safety and the BEPU approach are introduced; second, the statistical methodology chosen for the uncertainty and sensitivity analysis is explained. On the other hand, Chapter 6 covers the results of Paper IV, where a best-estimate simulation of a postulated station blackout scenario is performed with the modified version of CATHARE for the JHR (based on the outcomes of Chapter 3), and it is complemented with an uncertainty and sensitivity study. In Chapter 7 the results of the current research are summarized, and potential, future developments of the work are indicated.

Chapter 2

Fundamentals of thermal-hydraulics

Nuclear reactor cores such as the JHR usually consist of parallel fuel assemblies where an upward coolant flow is forced by a system of pumps. The coolability of the core shall be assured over a wide spectrum of conditions, with sufficient margins. In fact the power generated via nuclear fission reactions needs to be efficiently removed under normal operations, so that overheating is avoided and the integrity of the fuel elements is maintained without release of radioactive fission products. Adequate cooling capabilities shall also be provided in abnormal conditions, e.g. in the case of a loss of flow or coolant. Therefore accurate simulation models for single- and two-phase flow and heat transfer, are important for the analysis of the reactor behavior.

In this chapter the principles of thermal-hydraulics relevant to the thesis are presented. In particular, the mechanisms of heat transfer and boiling in a vertical channel (Section 2.1) and the onset of flow instability (Section 2.2) are described.

2.1 Two-phase flow and heat transfer in vertical channels

In a vertical channel with a forced, turbulent sub-cooled flow at the inlet and with a uniform heat flux at the wall, different flow and heat transfer regimes can be identified, as shown in Figure 2.1.

In the lower part of the channel, the heat transfer is governed by single-phase forced convection. The liquid and wet wall temperatures increase progressively with the axial elevation. At the Onset of Nucleate Boiling (ONB), small bubbles are generated in the micro-cavities (or nucleation sites) of the heated wall, and sub-cooled boiling begins. The small bubbles do not detach from the surface, since the bulk of the flow is sub-cooled. Thus, the void fraction remains close to zero. Nevertheless, the vaporization of the liquid in the micro-cavities causes an improvement of the heat transfer, which gradually shifts from single-phase forced convection to fully developed boiling (FDB). The forced convection and the nucleate boiling mechanism coexist during this phase, and the heat transfer regime is usually called 'partial boiling'.

The size of the bubbles grows along the channel, until they reach a critical value at which they can detach from the walls. As a consequence, the void fraction rapidly grows large. This point is known as Net Vapor Generation (NVG) or Onset of Significant Void (OSV).

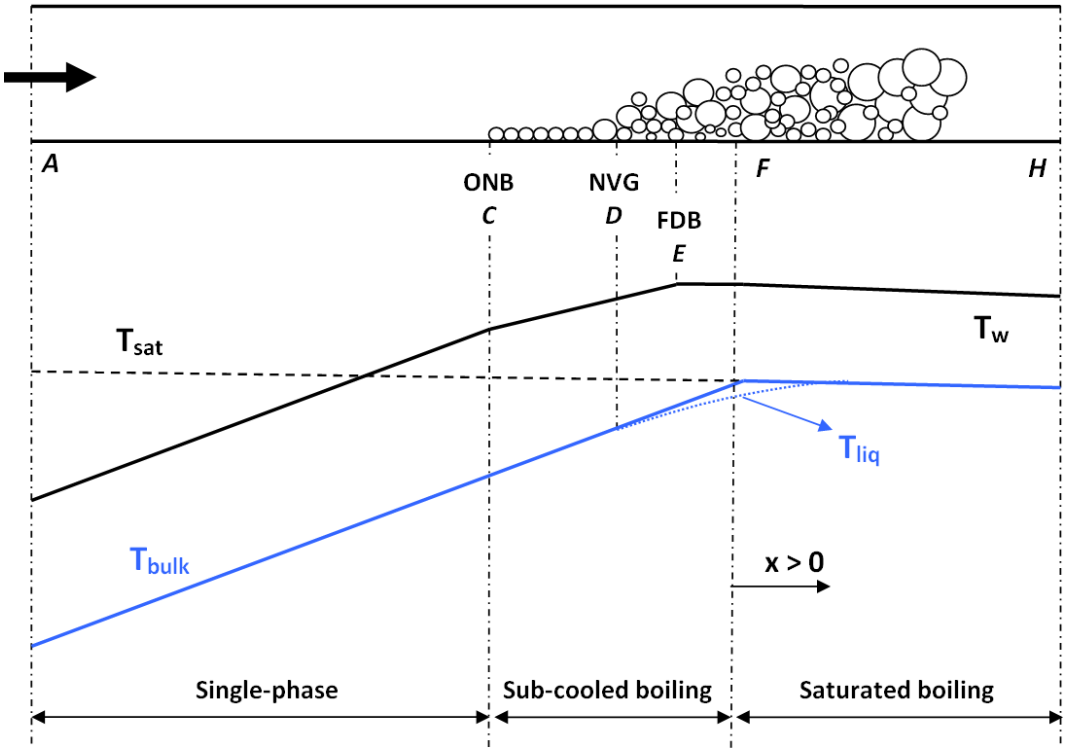

Figure 2.1: Boiling heat transfer in a vertical channel.

More and more vapor is produced in the channel, so the void fraction keeps increasing, and the flow pattern changes from bubbly to slug, and finally to annular. The saturated boiling starts when the flow reaches saturation conditions (i.e. steam quality x larger or equal to 0), and the heat transfer mechanism is very similar to the one in FDB. However, the heat transfer may be enhanced in annular flow because the liquid film in contact with the wall moves at high velocity [4].

The thickness of the liquid film in annular flow eventually goes to zero due to evaporation. Then the vapor comes into direct contact with the heated wall, causing a deterioration of the heat transfer and a sudden increase of the wall temperature. This phenomenon is named dry-out, and the corresponding heat flux is referred to as Critical Heat Flux (CHF).

Another condition in which critical heat flux can be reached, is the so-called Departure from Nucleate Boiling (DNB). Accordingly, although the bulk coolant temperature is below saturation, a stagnant vapor layer can locally form at the heated wall and prevent a proper cooling.

In nuclear reactors, operations must be conducted with a sufficient margin to CHF. In fact, the drastic temperature increase of the heated surface following a boiling crisis can damage the nuclear fuel elements and radioactive material can leak out. The prediction of the CHF conditions is therefore an important aspect for safety purposes.

For systems with parallel channels and single-phase liquid flow as the JHR, one potential scenario that can trigger CHF is the onset of flow instabilities, as discussed in the next section.

2.2 Onset of flow instability

The instabilities in two-phase flow can be static or dynamic [5]. A static instability is related to a small disturbance in the flow that induces the system to reach a steady state far from the initial one, or a periodic behavior. Such phenomena can be predicted using steady-state laws. For the dynamic instabilities, the flow inertia and thermal-hydraulic feedbacks are important, so the analysis requires the modeling of the dynamic behavior of the system.

The Flow Excursion (FE) [6] is a static instability that can cause a sudden decrease of the mass flow rate in a heated channel, with the danger of a possible boiling crisis. This type of phenomenon is also known as Ledinegg instability or Onset of Flow Instability (OFI). The condition for its occurrence arises when the slope of the curve pressure drop - mass flux for the external supply system (e.g., imposed by a pump characteristic) becomes larger than the one for the internal channel demand:

$$\left.\frac{\partial \Delta p}{\partial G}\right|_{Supply} \geq \left.\frac{\partial \Delta p}{\partial G}\right|_{Demand} \tag{2.1}$$

The OFI mechanism can be understood from Figure 2.2. The typical demand curve of a heated channel has an S-shape, and it is shown with the blue line. The supply curve for a system of parallel channels is flat (red line), because the total pressure drop is approximately constant. The operating conditions are then determined by the intersection between the two curves.

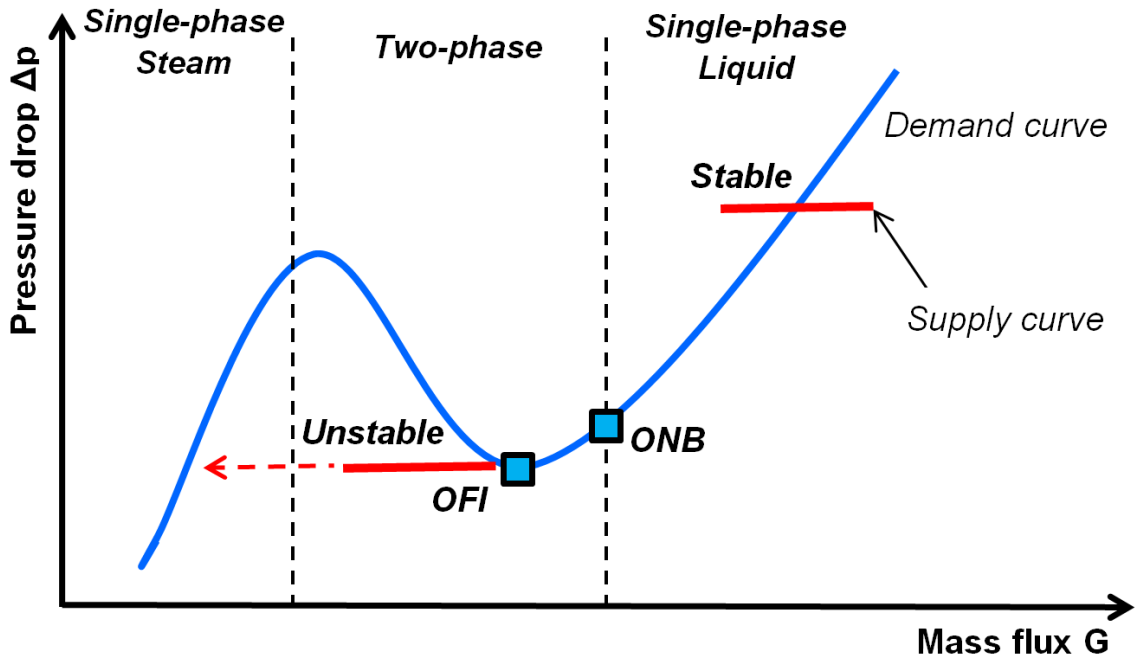

Figure 2.2: Onset of Flow Instability for heated parallel channels.

In the single-phase liquid region, the mass flux is sufficiently high and the system is stable, since the slope of the supply curve is smaller than the one of the demand curve. At lower values of mass flux, the channel reaches the Onset of Nucleate Boiling

(ONB). Nevertheless, the slope of the demand curve remains positive since the void fraction is negligible. Again, the operating point is stable.

Reducing further the mass flux, the Net Vapor Generation occurs and the void fraction starts to grow significantly. During this phase, the slope of the S-curve decreases due to the impact of the vapor on the pressure drop, until it becomes zero in connection with a minimum. The onset of flow instability can be then identified by determining such a minimum, since the slope of the supply curve is also zero. Therefore, the NVG slightly precedes the OFI [7, 8, 9], so that it is often referred to as a conservative indicator of the flow redistribution instability. In fact, although a rapid increase of void fraction begins from the NVG point, a large part of the channel is still in single-phase, stable conditions. In addition, the NVG is governed by local conditions, such as local pressure and heat flux, while the OFI is a global phenomenon which also depends on the geometry of the channel, e.g. the length-to-diameter ratio, and the type of supply curve.

At the OFI point, being the imposed pressure drop constant, a decrease of the mass flux leads to a sudden flow redistribution, since the only possible stable operating point is on the single-phase steam curve, where the slope of the S-curve is positive. During the flow redistribution transient, the rapid increase of void fraction determines an increase of the channel resistance. The latter causes a further reduction of the mass flow rate and therefore an enhancement of the void production, following a positive feedback. The flow excursion can thus trigger the occurrence of the critical heat flux.

Chapter 3

Thermal-hydraulic correlations and modifications of CATHARE

The system code CATHARE (Section 3.1) is applied to study the thermal-hydraulic behavior of the JHR in transient conditions. In order to investigate the reliability of the predictions, the correlations implemented in the code and possible alternatives are assessed for channels and conditions that are representative of the JHR. For this purpose, the SULTAN-JHR experiments are used (Section 3.2). The assessment studies discussed in Paper I and Paper II are focused on correlations for single-phase turbulent friction, single-phase turbulent heat transfer, fully developed boiling heat transfer and critical heat flux. The results together with the recommendations for the JHR modeling are summarized in Section 3.3. Additional modifications of CATHARE for the single-phase laminar flow and the laminar-turbulent transition, are discussed in Section 3.4.

3.1 The system code CATHARE

CATHARE has been developed since 1979 by the French Alternative Energies and Atomic Energy Commission (CEA), the French utility EdF, the reactor vendor AREVA-NP and the French Nuclear Safety Institute (IRSN) for the safety analysis of nuclear reactors. The code [3, 10] was originally meant for the simulation of transients in LWRs. Recently, its applicability has been also extended to the Sodium-cooled Fast Reactor (SFR), the Gas-cooled Fast Reactor (GFR), the Supercritical Light Water Reactor (SLWR), the Lead-cooled Fast Reactor (LFR), and to non-nuclear systems (e.g., cryogenic rocket engines).

The code is based on a 2-fluid 6-equations model for two-phase flow, complemented with appropriate closure laws for mass, momentum, and energy exchanges between liquid and vapor and between each phase and the wall. Additional models are included for the transport of non-condensable gases and radio-chemicals. Accordingly, CATHARE can be used to analyze complex systems that involve two-phase flow and boiling, thermal and mechanical non-equilibrium phenomena.

Different predefined modules can be combined to create the nodalization of a system: 0-D two-node modules are for large-sized volumes with several connections as

the plena in a reactor vessel; 1-D modules are for generic pipes and cooling channels; 3-D modules are for volumes where multi-dimensional flow effects are relevant.

The conservation equations are spatially discretized using a first-order upwind scheme and a staggered mesh. As regards the time-dependent problem, a fully implicit scheme is applied in the case of 0-D and 1-D modules, while the scheme for 3-D modules is semi-implicit. The set of discretized non-linear equations is finally solved with a Newton-Raphson iterative method.

A more detailed description of the code can found in [11].

In the next subsections, the correlations used in CATHARE, that are of interest in the current work, are presented.

3.1.1 Single-phase wall friction

The single-phase friction factor is used in the momentum conservation equation and is necessary for determining the pressure drop along a flow channel. In CATHARE the Fanning friction factor f is given as the maximum between three values, i.e.:

$$f = max\left(\frac{16}{Re}, \frac{0.079}{Re^{0.25}}, 0.003\right) \tag{3.1}$$

The first one is calculated with a relationship for laminar flow. The second expression relies on Blasius correlation [12], which is valid for turbulent flows in smooth pipes and for Reynolds number between 4000 and 10^5. Finally, the friction factor is set equal to 0.003 at high Reynolds numbers (larger than 4.81×10^5), mimicking the behavior of Moody's diagram.

3.1.2 Single-phase wall heat transfer

The energy equation requires the modeling of the heat transfer from the wall to the flow. In single-phase convection, the heat transfer is defined according to:

$$q''_{conv} = h_{conv}\Delta T \tag{3.2}$$

where h_{conv} is the convective heat transfer coefficient and ΔT is the temperature difference between the wall and the bulk of the coolant.

In CATHARE the heat transfer coefficient is obtained as the maximum of 4 different values:

$$h_{conv} = max\ (h_{lam,NC};\ h_{turb,NC};\ h_{lam,FC};\ h_{turb,FC}) \tag{3.3}$$

where the coefficients for laminar natural convection $h_{lam,NC}$, turbulent natural convection $h_{turb,NC}$, laminar forced convection $h_{lam,FC}$, and turbulent forced convection $h_{turb,FC}$ are used. These coefficients are determined using empirical relationships and are expressed in terms of the Nusselt number.

The heat transfer coefficients in laminar and turbulent natural convection are, respectively:

$$Nu_{lam,NC} = 0.55(Ra)^{1/4} \tag{3.4}$$

$$Nu_{turb,NC} = 0.13(Ra)^{1/3} \tag{3.5}$$

Under forced flow conditions, the heat transfer coefficient in laminar flows is constant and does not depend on the Reynolds and Prandtl numbers [13]. In CATHARE, the following relationship is used:

$$Nu_{lam,FC} = 3.66 \tag{3.6}$$

The turbulent forced-convection heat transfer coefficient is modeled with the Dittus-Boelter correlation [14]:

$$Nu_{turb,FC} = 0.023 Re^{0.8} Pr^{0.4} \tag{3.7}$$

The equation above was derived for circular pipes, but its application may be extended to other geometries with the use of the hydraulic diameter [13]. The correlation is applicable for $0.7 < Pr < 120$, $10000 < Re < 1.24 \cdot 10^5$ and $L/D_{hydr} > 60$.

3.1.3 Two-phase wall heat transfer

The two-phase heat transfer modeling of CATHARE is based on a modified version of Bowring model for sub-cooled boiling [15]. The heat transfer is thus described by a superposition of effects. The total heat flux imposed at the wall (ϕ), is divided into two parts: one part heats up the liquid phase (q''_{wl}) and the other one vaporizes the liquid at the liquid-vapor interface (q''_{wi}). Accordingly, the following relationship can be written:

$$\phi = q''_{wl} + q''_{wi} \tag{3.8}$$

Depending on the heat transfer mechanism, the two terms are modeled as:

- Sub-cooled boiling:

$$T_l < T_{sat} < T_w \quad \Longrightarrow \quad \begin{cases} q''_{wl} = q''_{conv} + (1-\epsilon) q''_{nb} \\ q''_{wi} = \epsilon q''_{nb} \end{cases} \tag{3.9}$$

- Saturated boiling:

$$T_l > T_{sat} \quad \Longrightarrow \quad \begin{cases} q''_{wl} = 0 \\ q''_{wi} = q''_{nb} \end{cases} \tag{3.10}$$

In the saturated boiling region, bubbles are generated at the wall and move to the bulk of flow (see Section 2.1), so the nucleate boiling is the predominant heat transfer mechanism. The associated heat flux in CATHARE is calculated as:

$$q''_{nb} = 1.97 \cdot 10^3 \; e^{\left(2.3 \cdot 10^{-7} p\right)} \left(T_w - T_{sat}\right)^2 \tag{3.11}$$

and it is entirely used to vaporize the liquid in agreement with Eqn. (3.10).

This expression for the nucleate boiling term is derived from Thom correlation [16], that is valid for fully developed boiling and is expressed in terms of wall superheat as:

$$\Delta T_{sat} = 22.65 \left(\frac{\phi}{10^6}\right)^{0.5} e^{\left(-\frac{1}{87}\frac{p}{10^5}\right)} \tag{3.12}$$

This relationship was developed for a vertical tube with a diameter of 12.7 mm, upward water velocities between 1.5 and 6.1 m/s, pressures between 5.17 and 13.78 MPa, and heat fluxes between 0.284 and 1.58 MW/m^2.

The sub-cooled boiling involves formation of bubbles at the wall, while the bulk of the flow is still sub-cooled. Then single-phase convection and nucleate boiling co-exist at this stage. Correspondingly, the model (3.9) is a combination of Eqn. (3.2) and Eqn. (3.11), where the parameter ϵ gives the rate of vaporization (see details in [17]). The explicit treatment of the ONB and FDB points is disregarded. Such a simplification is for the benefit of a more robust code structure, without any major impact on the performances as shown in [17]. As a consequence, the transition from liquid single-phase convection to sub-cooled boiling, is approximated with the NVG point. The latter is identified using a modified version of the Saha-Zuber correlation [18] that was developed at CEA-Grenoble [19] using KIT experiments [20]. The correlation provides the liquid sub-cooling at NVG and it reads as:

$$\Delta i_{sub,NVG} = \begin{cases} 5\frac{\phi \ c_{p,l} \ D_{hydr}}{455 \ k_l} & \text{if } Pe < 0.52 \ Pe_0 \\ 2\frac{\phi \ c_{p,l} \ D_{hydr}}{65\cdot 10^{-4} \ k_l \ Pe_0 \ \left(\frac{Pe}{Pe_0}\right)^{1.4}} & \text{if } Pe \geq 0.52 \ Pe_0 \end{cases} \tag{3.13}$$

where $Pe_0 = 7 \cdot 10^4$. The validity range is such that: $340 < G < 2100$ kg/m^2/s, $4.4 < p < 11$ MPa and $0.43 < \phi < 1.72$ MW/m^2. Also, the FDB is assumed to occur when T_l is equal to T_{sat}, even though it physically starts slightly earlier.

3.1.4 Critical Heat Flux

As discussed in Section 2.1, the CHF corresponds to a sudden deterioration of the heat transfer coefficient, which causes a sharp increase in wall temperature and eventually burnout.

In CATHARE, the 1986 AECL-UO Groeneveld lookup tables [21] are employed. These tables were derived from more than 15000 CHF experiments in circular pipes. They are valid for an 8-mm tube and they are arranged as a function of pressure, mass flux and steam quality. To evaluate the CHF at flow conditions different from the ones in the tables, cubic spline interpolations are used. For hydraulic diameters different from 8 mm, the interpolated values are corrected as:

$$\phi_{CHF,Groeneveld} = \phi_{CHF,interp}(p, G, x, D_{hydr} = 8mm) \cdot K_{D_h} \tag{3.14}$$

The factor K_{D_h} is equal to:

$$K_{D_h} = \begin{cases} \left(\frac{8}{D_{hydr}}\right)^{\frac{1}{3}} & \text{if } 2 \text{ mm} < D_{hydr} < 16 \text{ mm} \\ \left(\frac{8}{16}\right)^{\frac{1}{3}} = 0.79 & \text{if } D_{hydr} \geq 16 \text{ mm} \end{cases} \tag{3.15}$$

Other corrections, implemented in CATHARE, are not reported here because they are not applicable to this work.

The applicability range of the table in CATHARE is: $0.2 < p < 20$ MPa; $0 < G < 7500$ kg/m^2/s; and $-0.15 < x < 1$, with the negative quality referring to sub-cooled conditions.

3.2 The SULTAN-JHR experiments

The SULTAN-JHR experimental program was carried out at CEA Grenoble (France) during the years 2001-2008. The main objective was to obtain a reliable set of data for the validation of CATHARE with respect to the JHR core. Thus, the test sections were designed with geometrical characteristics (i.e. gap sizes and hydraulic diameters) and system conditions (see Table 3.1) representative of the JHR core channels. The rectangular geometry was chosen to simplify the manufacturing process and to have a high geometric precision. The curvature of the JHR fuel plates is expected to have a small influence on the flow and the heat transfer, mainly in terms of a reduced lateral mixing as observed in this kind of geometry [22, 23].

Table 3.1: System conditions in the SULTAN-JHR experiments.

Outlet pressure [MPa]	$0.2 - 0.9$
Inlet water temperature [°C]	$25 - 160$
Mass flow rate [kg/s]	$0.05 - 2.0$
Flow velocity [m/s]	$0.5 - 18$
Uniform heat flux [MW/m^2]	$0.5 - 7.5$

3.2.1 Test section

The test section consists of a narrow rectangular channel that is delimited by two Inconel-600 plates, as shown in Figure 3.1. A direct electrical current is applied to the plates in order to heat the channel.

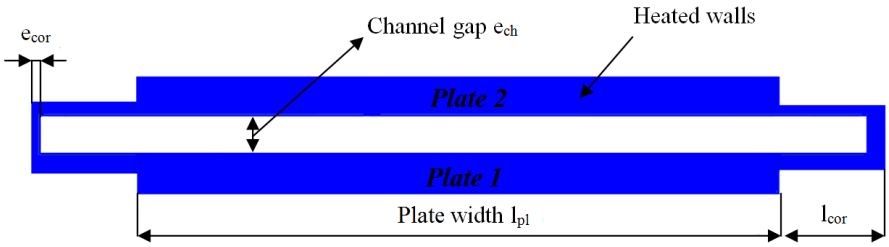

Figure 3.1: Top view of the SULTAN-JHR test section.

The extremities of the walls are thinner to avoid heat concentration effects that might cause higher heat fluxes at the corners, with undesirable boiling and thermal crisis [24]. The test section is surrounded by an electrical mica-based insulation (*Cogetherm*®), and by two 25 mm thick pressure steel plates that are meant to maintain the geometry of the channel unchanged during the experiments. Finally, a 200 mm thick rock wool layer is placed on the external side to reduce heat losses.

The axial geometry and the instrumentation layout of the test section is displayed in Figure 3.2. The channel consists of 3 axial regions. The central part, whose length is approximately 600 mm, is heated and the power is transferred from the walls to the fluid. On the other hand, the entrance and the exit zones are adiabatic and they are 70 mm long. The inlet of the test section is smooth in order to minimize possible entrance effects; conversely, the outlet is abrupt.

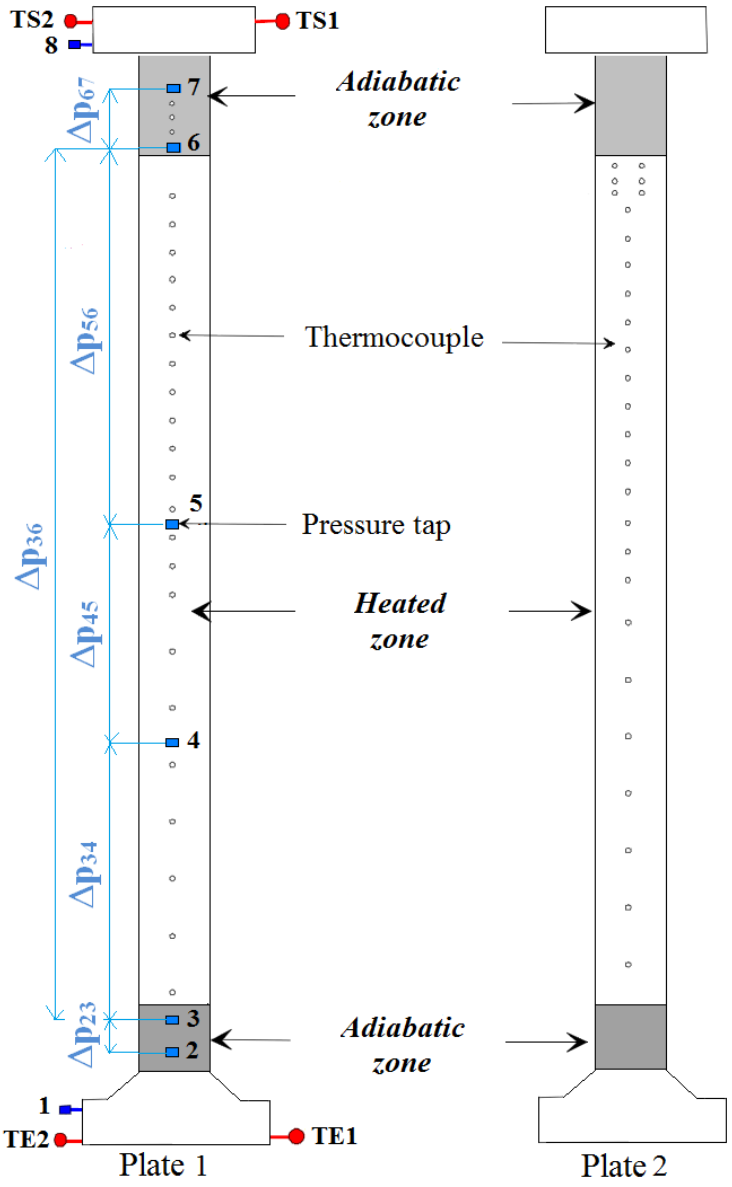

Figure 3.2: Axial geometry and instrumentation layout of the SULTAN-JHR test section.

Three different test sections were used: Section 3 (SE3) with channel gap equal to 1.509 mm and uniform heat flux; Section 4 (SE4) with channel gap equal to 2.161 mm and uniform heat flux; and Section NU with channel gap equal to 1.540 mm and non-uniform heat flux. The geometrical details of the test sections are reported in Table 3.2. Section NU is similar to SE3, however the thickness of the plates is not constant. In fact, it increases linearly from 1.0 mm at mid-elevation to 1.66 mm at the extremities, so that a non-uniform axial heat flux profile with a peak at the center, could be obtained. The ratio between the local and average heat flux varies approximately from 0.8 to 1.25, as shown in Figure 3.3.

The tests are performed with forced, upward flow of demineralized and degassed water (except in the case of the tests with dissolved gas).

Additional details related to the SULTAN-JHR experiments can be found in [17].

Table 3.2: Test section geometry (dimensions in mm).

	SE3	**SE4**	**NU**
Gap size (e_{ch})	1.509 ± 0.040	2.161 ± 0.050	1.540 ± 0.050
Heated height (H_{ch})	599.8 ± 0.1	599.7 ± 0.1	599.8 ± 0.1
Plate width (l_{pl})	47.2 ± 0.1	47.15 ± 0.1	47.0 ± 0.1
Length of the corners (l_{cor})	3.15 ± 0.1	2.85 ± 0.1	3.0 ± 0.1
Thickness of the corners (e_{cor})	0.5	0.5	0.5
Averaged thickness of plate 1 ($\bar{e}_{pl1}$)	1.0087 ± 0.006	1.003 ± 0.002	Varying
Averaged thickness of plate 2 ($\bar{e}_{pl2}$)	0.9818 ± 0.018	1.004 ± 0.002	Varying

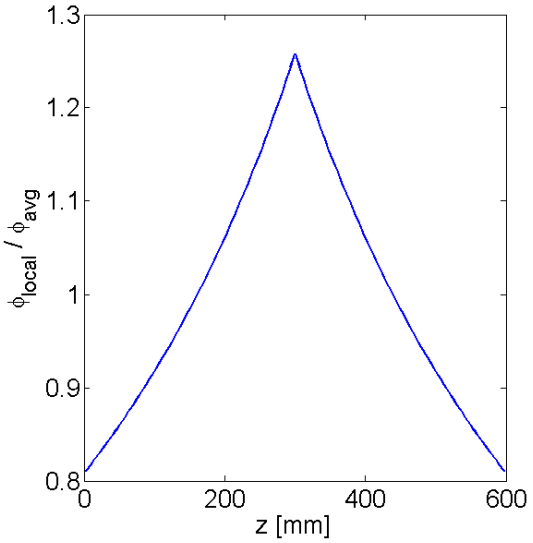

Figure 3.3: Axial heat flux profile in the test section NU.

3.2.2 Instrumentation

The facility was instrumented in such a manner that the following parameters could be recorded: mass flow rate, water temperature, absolute pressure, pressure drop, dry wall temperature, electrical current and voltage. Two venturi tubes in parallel, placed before the test section, were used to measure the mass flow rate. The water temperature was measured at the entrance of the test section (TE1 and TE2 in Figure 3.2) and at the exit (TS1 and TS2). The pressure taps were placed at 8 axial locations on plate 1 (blue squares in Figure 3.2), and 6 pressure drops were recorded, namely Δp_{23}, Δp_{34}, Δp_{45}, Δp_{56}, Δp_{67}, and Δp_{36}. The dry wall temperature was detected with 42 insulated K-thermocouples positioned along the heated channel, in the insulation layer (circles in Figure 3.2). The wet wall temperature was then derived via an experimental data reduction (see details in Paper I). In addition, 19 non-isolated K-thermocouples (not shown in Figure 3.2) were available at the end of the heated zone for the rapid detection of CHF (see Paper II). The power supplied to the test section was evaluated from the measured voltage ΔV and current I, as $P = \Delta V \cdot I$.

3.2.3 Test procedures

A database of 605 experiments was built and includes isothermal tests, flow redistribution tests, CHF tests, and tests with dissolved gas in the flow.

There are 149 isothermal experiments performed without any power input and they are important for the validation of models of friction.

As regards flow redistribution, there are 120 experiments in test section SE3, 133 in SE4, and 125 in NU. The procedure was such that the outlet pressure, power and inlet temperature were fixed, while the mass flow rate was reduced in steps. Then, the pressure drop along the channel could reach the minimum that identifies the onset of flow instability (see also the discussion in section 2.2). For each step, sufficient time was waited to stabilize the conditions and take steady-state measurements. These experiments can also be used for the assessment of the correlations in single-phase forced convection and in fully developed boiling.

A number of 46 tests were carried out to investigate the thermal crisis limits (CHF). For these tests, the pressure at the exit, the heat flux and the mass flow rate were kept constant, and the temperature at the entrance was increased by 0.2 °C/min. The thermal crisis could be determined by the rapid increase of temperature from the rapid detection thermocouples.

The 32 nitrogen-saturated tests were conducted in SE4 and aimed to study the influence of dissolved gases on the OFI point. The same procedure as the one followed in the flow redistribution experiments was applied.

3.2.4 Simulation of the experiments

The SULTAN-JHR experiments are simulated with CATHARE, so that the correlations of interest can be assessed. The test section is modeled as a 1-D channel with hydraulic diameter derived from the data reported in Table 3.2. The heated region is discretized with 150 axial computational volumes of 4 mm each, and the mesh independence of the results is proven [17]. This nodalization is chosen in such a manner that the center of the volumes corresponds to the position of the thermocouples and pressure taps.

Furthermore, to simplify the procedure for the assessment of the single-phase turbulent heat transfer coefficient, a specific model is developed in Matlab. The same nodalization as in CATHARE is used, but uniform heat flux boundary condition replaces the CATHARE modeling of the heated walls. The estimation of the bulk liquid temperature is based on a heat balance, which gives the fluid enthalpy i_l as a function of the axial distance z:

$$i_l(z) = i_l(z=0) + \frac{\phi P_{wet}}{\dot{m}} z \tag{3.16}$$

The pressure drops are calculated according to the following expression:

$$\Delta p = \Delta p_{grav} + \Delta p_{fric} + \Delta p_{acc} \tag{3.17}$$

Since only single-phase flows are analyzed with this model, the acceleration term in Eqn. (3.17) can be neglected. In fact, the latter is much smaller than the total pressure drop ($\Delta p_{acc} < 10^{-4} \cdot \Delta p$). The gravity and the friction terms read respectively as:

$$\Delta p_{grav} = \rho_l g \Delta z \tag{3.18}$$

$$\Delta p_{fric} = 4f \frac{\Delta z}{D_{hydr}} \frac{G^2}{2\rho_l} \tag{3.19}$$

3.3 Assessment of correlations

3.3.1 Single-phase turbulent friction

In rectangular channels, the Blasius relationship implemented in CATHARE underestimates the friction factor (magenta line in Figure 3.4).

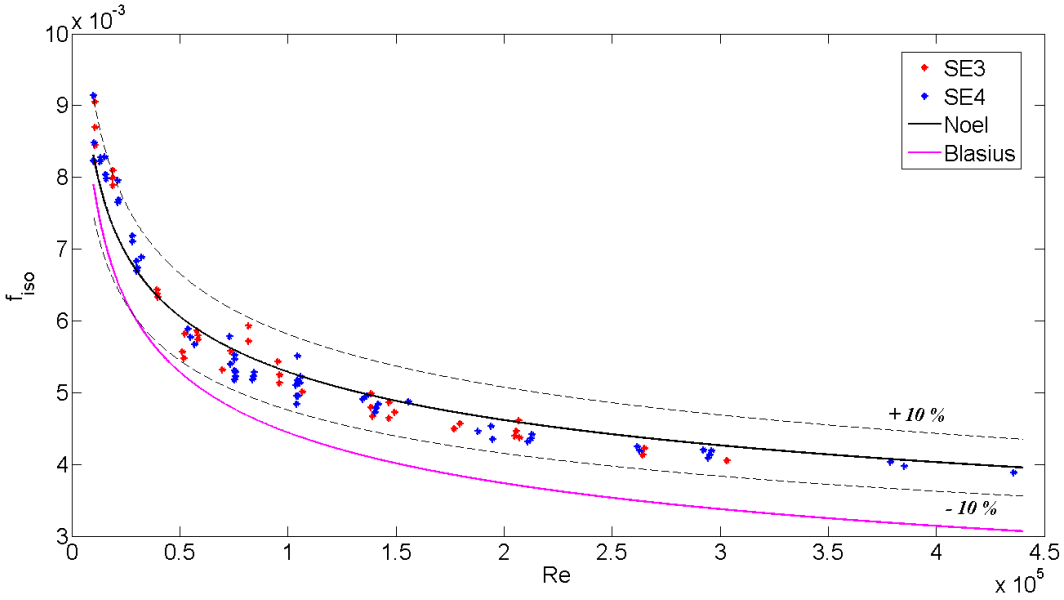

Figure 3.4: Experimental isothermal friction factor as a function of the Reynolds number.

A correlation was therefore developed by Noel using the SULTAN-JHR experiments in isothermal conditions (black line in Figure 3.4), and it reads as:

$$f_{iso,turb} = \frac{0.0505}{Re^{0.196}} \tag{3.20}$$

For the non-isothermal case, a corrective factor F_{cor} is applied, i.e.

$$f_{turb} = F_{cor} \times f_{iso,turb} \tag{3.21}$$

$$F_{cor} = 1 - \frac{P_{heat}}{P_{wet}} \frac{0.0085(T_w - T_l)}{1 + 2\left[\frac{T_w + T_l}{200}\right]^{1.5}} \tag{3.22}$$

This corrective factor takes into account the influence of the heat flux on friction, and it is a modified version of Costa correlation [25] developed internally at CEA. The performance of these correlations against the heated tests is shown in Figure 3.5. It includes a total number of 95 tests with Reynolds numbers between 1.0×10^4 and 3.1×10^5.

In the context of this thesis, the accuracy is also quantified: the discrepancies between experimental and calculated points are approximately distributed as a Gaussian with mean and standard deviations equal to 0.22 % and 5.64 %, respectively (see more details in Paper I).

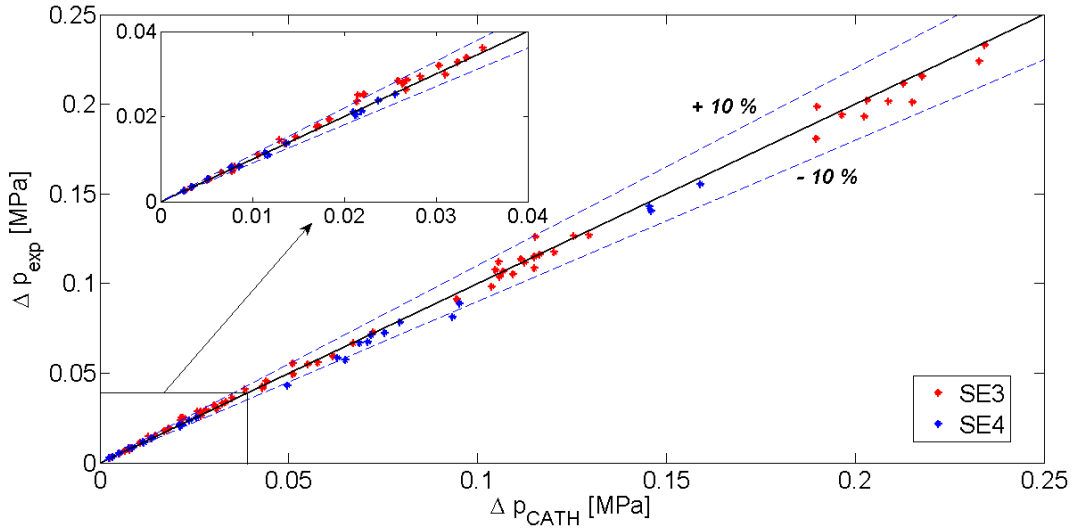

Figure 3.5: Comparison of the experimental pressure drops with CATHARE results obtained using the friction factor in Eqn. (3.21).

3.3.2 Single-phase turbulent heat transfer

The modeling of the single-phase turbulent heat transfer in narrow rectangular channels at high Reynolds numbers, has been investigated in a limited number of works [24, 26]. These studies were carried out in the 1960s and led to contradictory results. Due to the lack of experimental data, it is usually suggested to use standard correlations for circular pipes such as the Dittus-Boelter correlation (3.7), where the hydraulic diameter is introduced as characteristic length [13]. Recent publications [27, 28] pointed out that this kind of approach may under-predict the heat transfer, although narrow ranges of conditions and low Reynolds numbers (i.e. $Re < 13000$) were considered.

One of the objectives of the SULTAN-JHR campaign was therefore to provide experiments for the assessment of correlations for single-phase turbulent heat transfer over a wider range of conditions. In particular, a large number of experimental points was collected (1723 with the test section SE4, and 1036 with SE3), for Reynolds numbers between 1.0×10^4 and 2.69×10^5 and Prandtl numbers between 1.18 and 5.94.

For the purpose of the assessment, the experimental Nusselt number is defined as:

$$Nu_{exp} = \frac{h_{exp} D_{hydr}}{k_l} \tag{3.23}$$

where the experimental heat transfer coefficient reads as:

$$h_{exp} = \frac{\phi}{(T_w - T_l)} \tag{3.24}$$

The comparison with the SULTAN-JHR experimental data shows that the Dittus-Boelter correlation (i.e. the standard model in CATHARE) significantly under-estimates the heat transfer coefficient, especially at high Reynolds number (see Figure 3.6).

Similar results were obtained with other correlations developed for circular pipes (e.g. Sieder-Tate [29]), as discussed in Paper I.

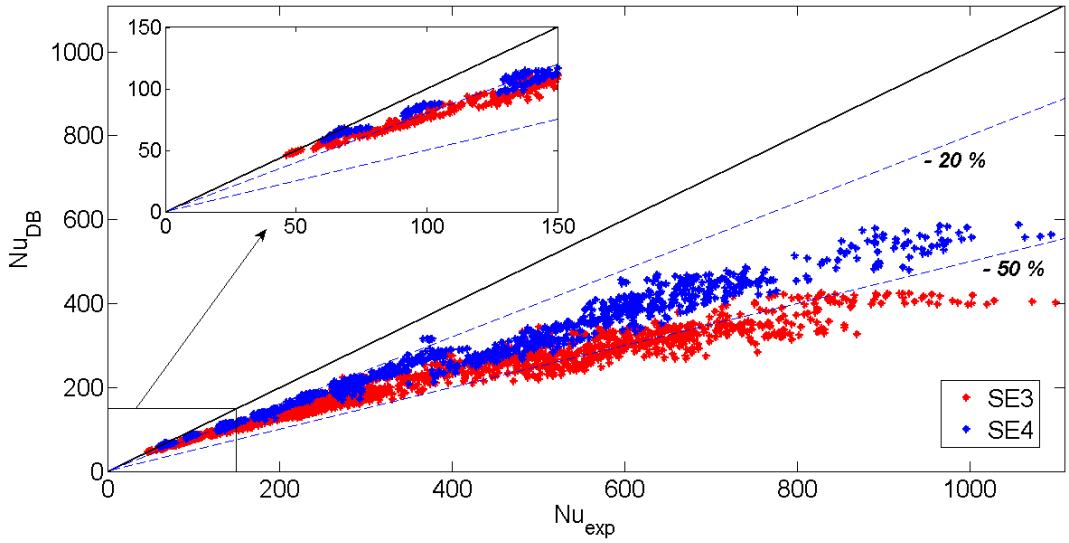

Figure 3.6: Comparison of the experimental data with Dittus-Boelter correlation.

3.3.2.1 Development of correlations based on the SULTAN-JHR data

In order to provide a more realistic model for the JHR case, new correlations are developed from the best-fitting of the SULTAN-JHR data. The Seider-Tate structure of the correlation is selected:

$$Nu = aRe^{b_{Re}} Pr^{c_{Pr}} \left(\frac{\mu}{\mu_w}\right)^{0.14} \tag{3.25}$$

This form was preferred to the Dittus-Boelter one, since better predictions can be achieved at high heat fluxes by including the viscosity ratio. The coefficients of Eqn. (3.25) are optimized using a multiple linear regression approach. This procedure is applied to the data for SE3 and SE4 separately.

The best-fitting correlation for SE4 reads as:

$$Nu = 0.0044Re^{0.960} Pr^{0.568} \left(\frac{\mu}{\mu_w}\right)^{0.14} \tag{3.26}$$

The coefficient of determination R^2, which indicates the goodness of fit, is equal to 0.995 and the performance of the correlation with respect to the experimental data is shown in Figure 3.7.

Assuming a normal distribution of the residuals obtained from the experimental and calculated Nusselt numbers, the mean and standard deviation are respectively 0.13 % and 5.02 % (see paper I).

The best-fitting correlation for SE3 reads as:

$$Nu = 0.00184Re^{1.056} Pr^{0.618} \left(\frac{\mu}{\mu_w}\right)^{0.14} \tag{3.27}$$

Similar performances to the ones for the case of SE4 are found, but with a larger standard deviation (equal to 8.36 %), as detailed in Paper I.

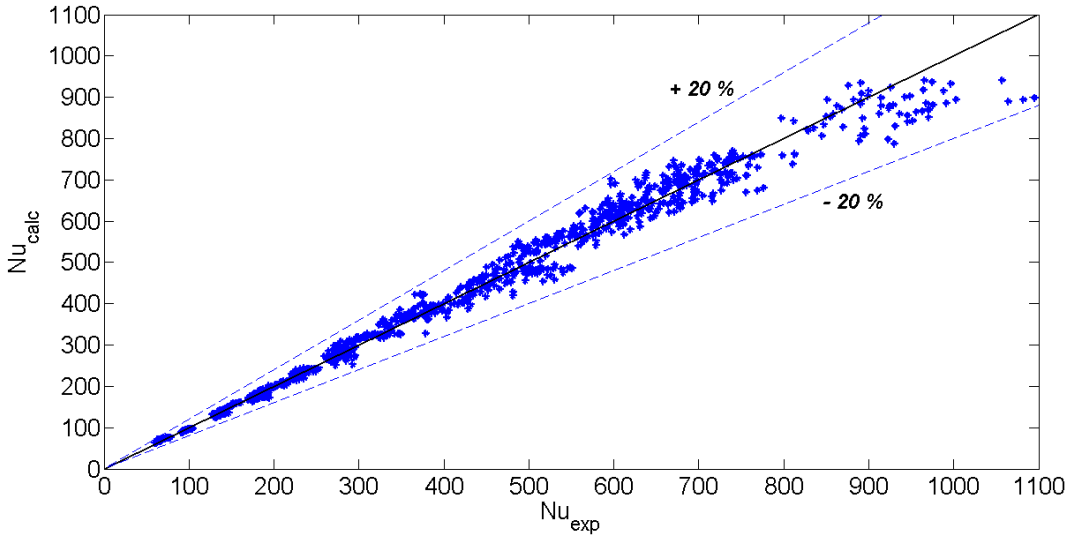

Figure 3.7: Comparison of SE4 experimental data with the best-fitting model (3.26).

For the modeling of the JHR, Eqn. (3.26) is suggested. In fact the gap size of the average JHR channel is 1.95 mm, and it is closer to the one of SE4 (2.16 mm). Furthermore, the width-to-gap ratio of the most internal channels of the JHR fuel assemblies is similar to the one of SE4 (equal to about 24). Finally, the correlation gives conservative values of the heat transfer coefficient when used for the most external channels whose width-to-gap ratio is higher.

3.3.2.2 Influence of the channel geometry

The comparison of the results in SE3 and SE4 reveals that the channel geometry can affect the heat transfer coefficient, as displayed in Figure 3.8.

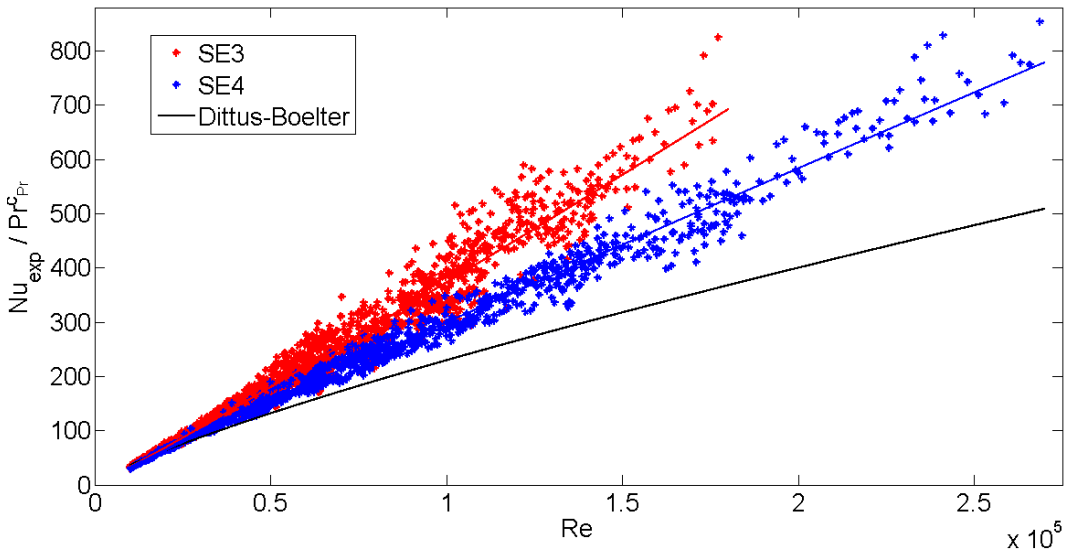

Figure 3.8: Nusselt number as a function of the Reynolds number.

The heat transfer coefficient is higher in SE3 that has the smaller channel gap. This suggests that an enhancement of the heat transfer may occur with the decrease

of the gap size. The discrepancies between the two test sections grow with the increase of the Reynolds number. In the figure, the experimental Nusselt number is divided by the Prandtl number to the power of the corresponding c_{pr} coefficient in order to better visualize the influence of the Reynolds number. For the sake of completeness, the lines representing correlations (3.26), (3.27) and (3.7) are also included in the plot. The comparison between the experimental data and Dittus-Boelter also emphasizes how this relationship may be considered to be accurate at low Reynolds numbers (less than 25000), but again the discrepancies increase with the Reynolds number.

3.3.3 Fully developed boiling heat transfer

Correlations for the prediction of the wall superheat in fully developed boiling are evaluated using the SULTAN-JHR experiments. As explained in Paper I, a careful review of the experimental database led to the selection of 32 tests performed in SE4, where FDB could be clearly identified. A total number of 227 experimental points was then collected. The range of conditions is reported in Table 3.3.

Table 3.3: Range of physical parameters of the FDB experimental points.

Pressure [MPa]	0.23 - 0.9
Mass flux [kg/m^2/s]	500 - 5364
Uniform heat flux [MW/m^2]	0.46 - 4.41
Liquid sub-cooling [°C]	0 - 38.5
Steam quality	-0.08 to 0.08

The relationship of Thom (3.12) used in CATHARE significantly under-predicts the FDB heat transfer, computing higher wall superheat in comparison with the experiments (Figure 3.9).

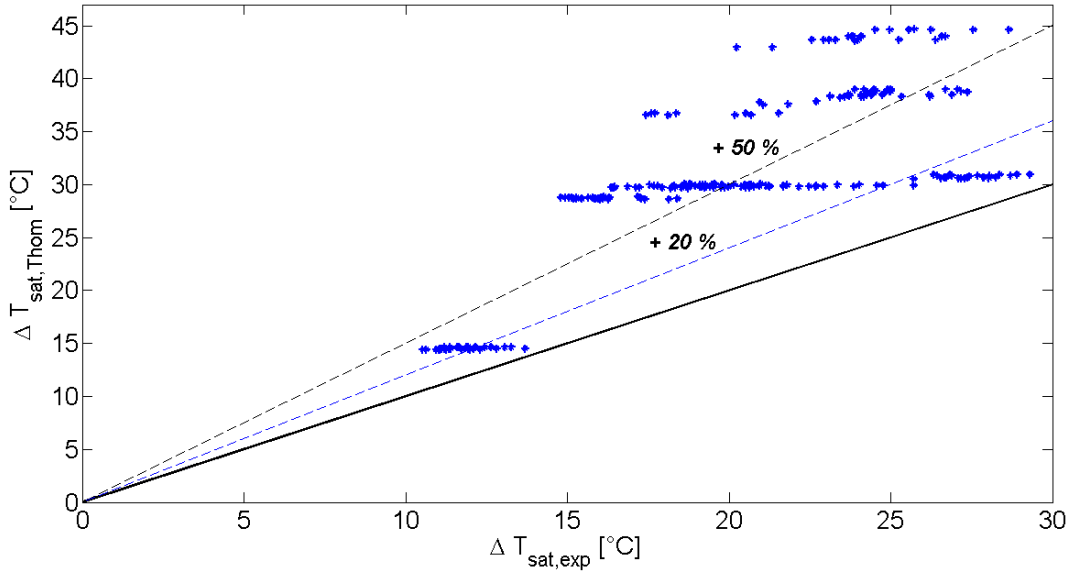

Figure 3.9: Comparison of the experimental data with Thom correlation.

Other FDB correlations have been also considered. However, only the results related to the Forster-Greif relationship are reported in this section, while the overall analysis can be found in Paper I.

The Forster-Greif correlation was originally developed from theoretical considerations complemented with a limited set of experimental data in pool boiling of water at pressures of 1 and 50 atm [30]. To overcome the complexity of the original relationship, simplified formulations have been derived. One of these simplified versions reads as:

$$\Delta T_{sat} = 4.57 \left(\frac{p}{10^5}\right)^{-0.23} \left(\frac{\phi}{10^4}\right)^{0.35} \tag{3.28}$$

The exclusive dependence of the wall superheat on the system pressure and the imposed heat flux (i.e. known quantities) makes this correlation very simple to use and implement in system codes.

The relationship has been applied to research reactors with fuel plates (e.g. [31]) and is verified in small-diameter tubes (between 2 and 4 mm), at high heat fluxes (between 5.6 and 20.5 MW/m^2), and low pressures (approximately between 0.13 and 0.5 MPa) [32]. A more comprehensive explanation is provided in [17].

The comparison with the SULTAN-JHR experimental data showed that this relationship can predict the wall superheat in a relatively accurate manner (Figure 3.10). The residuals can be approximately described by a Gaussian with mean and standard deviation equal to 1.3 % and 10.1 %, respectively (see details in Paper I). This correlation has been therefore implemented in CATHARE for the modeling of the JHR.

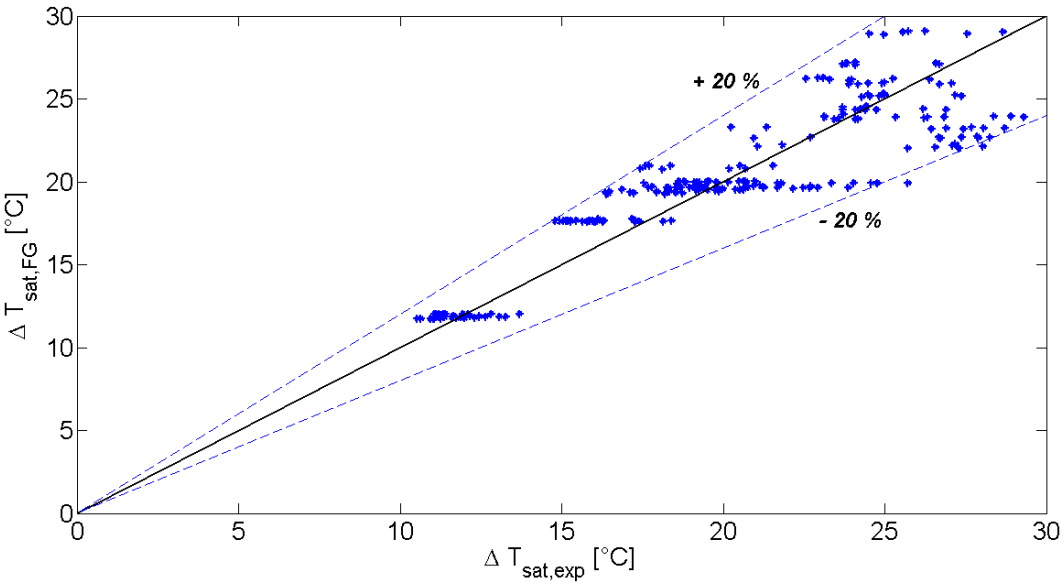

Figure 3.10: Comparison of the experimental data with Forster-Greif correlation.

3.3.4 Critical Heat Flux

In Paper II, selected CHF correlations are tested against the 46 CHF experiments available from the SULTAN-JHR campaign. The range of conditions of these tests is reported in Table 3.4.

Table 3.4: Range of physical parameters in the CHF tests.

Outlet pressure [MPa]	0.377 - 0.866
Mass flux [kg/m^2/s]	1178 - 6578
Inlet liquid sub-cooling [°C]	56.4 - 156.4
Outlet steam quality	-0.008 to 0.178

The results are presented in terms of Critical Heat Flux Ratio:

$$CHFR = \frac{\phi_{CHF,calc}}{\phi_{CHF,exp}} \tag{3.29}$$

A ratio smaller or equal to unity indicates that the correlation predicts the occurrence of the CHF.

The 1986 AECL-UO Groeneveld look-up table is the standard model in CATHARE (see Section 3.1.4). The CHFR calculated for the SULTAN-JHR experiments is always greater than 1 (Figure 3.11). Thus, the table provides a non-conservative estimation, since the real boiling crisis occurs at lower heat fluxes.

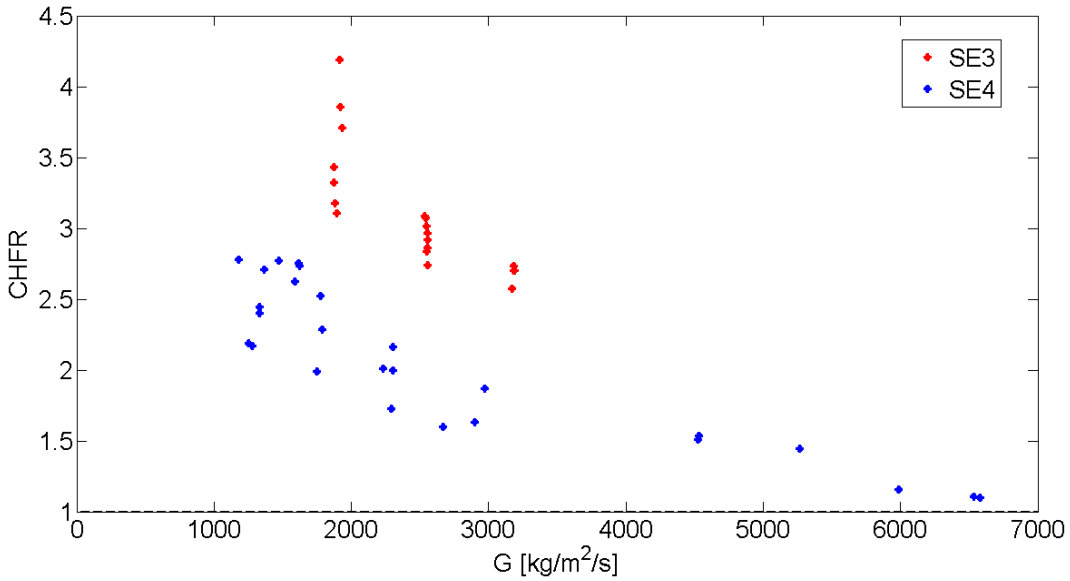

Figure 3.11: CHFR estimated with 1986 AECL-UO Groeneveld look-up table.

As discussed in Paper II, correlations that were developed for channels comparable to the SULTAN test sections, can give better results. For instance, a suitable option for the JHR is the Sudo correlation. It was derived for research reactors with plate-type fuel, using 596 experimental CHF points, both in up- and down-flow. The majority of the up-flow experiments were performed in bilaterally heated rectangular channels, with gap sizes equal to 2.25, 2.4 and 2.8 mm. The flow conditions are similar to the SULTAN-JHR ones, but with lower mass fluxes ($G < 600$ kg/m^2/s). Other experiments in unilaterally heated rectangular channels and squared ducts internally heated with a cylinder, were also used. In particular the validity range for the mass fluxes was extended to 6250 kg/m^2/s by including 8 CHF points from experiments in a unilaterally heated rectangular channel with width-to-gap ratio equal to 1.5.

The Sudo relationship is expressed in terms of the dimensionless local critical heat flux ϕ^*_{CHF}, the dimensionless mass flux G^*, and the dimensionless local sub-cooling

Δi^*_{sub}. In up-flow conditions, ϕ^*_{CHF} can be calculated as:

$$\phi^*_{CHF} = max\left(\phi^*_{CHF,1}; \phi^*_{CHF,3}\right) \tag{3.30}$$

$$\phi^*_{CHF,1} = 0.005|G^*|^{0.611}\left(1 + \frac{5000}{|G^*|}\Delta i^*_{sub}\right) \tag{3.31}$$

$$\phi^*_{CHF,3} = 0.7\frac{A}{S_{heat}}\frac{\sqrt{\frac{l_{heat}}{\lambda}}}{\left(1 + \left(\frac{\rho_g}{\rho_l}\right)^{0.25}\right)^2} \tag{3.32}$$

where $\phi^*_{CHF,3}$ represents the minimum CHF value in case of very low mass flux or counter-current flow.

As shown in Figure 3.12, the correlation performs reasonably well for SE4 with a mean error of -2 % and a standard deviation of 10 %, but over-predicts the SE3 experimental data with a mean error of 32 % and a standard deviation of 12 %.

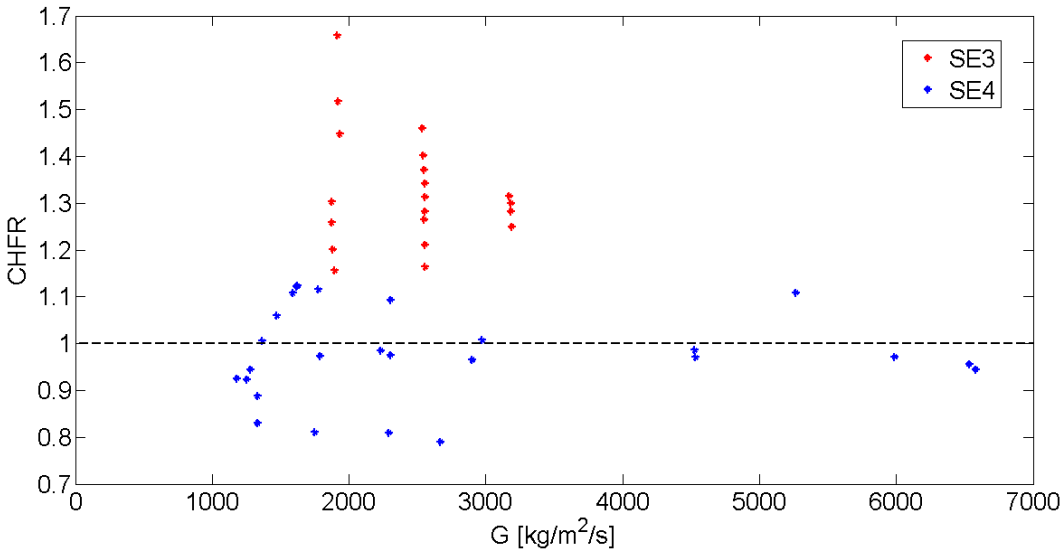

Figure 3.12: CHFR as a function of the mass flux using Sudo's correlation.

One of the possible reasons for such a difference is that the experiments used to develop the correlations are performed in channels that are closer to SE4. In fact the geometry may have an impact: a reduction of the gap size is expected to cause the CHF to decrease. However, the effect cannot be fully quantified due to the lack of experimental data.

3.4 Further modifications of CATHARE

In view of the analysis of the JHR, modifications are also introduced into CATHARE for the laminar flow and for the laminar-turbulent transition. These flow regimes are rarely encountered in normal operations of a reactor, but they may appear in accidental situations. Since very few experiments for these types of conditions are available from the SULTAN-JHR database, the modifications are mainly based on the literature.

3.4.1 Single-phase laminar friction

The relationship for the laminar friction factor in CATHARE is valid for circular ducts. A more suitable correlation that can be used for rectangular channels is the Shah-London correlation [33]. The latter reads as:

$$f_{iso,lam} = \frac{24}{Re} f(AR) = \frac{24}{Re}(1 - 1.3553AR + 1.9467AR^2 + \\ - 1.7012AR^3 + 0.9564AR^4 - 0.2537AR^5) \tag{3.33}$$

In this equation, the friction factor computed for two infinite vertical plates is corrected with the factor $f(AR)$ that depends on the aspect ratio AR (i.e., the ratio between the gap size and the channel width). The correction to the friction factor decreases with the increase of the aspect ratio, and it is equal to unity for infinite plates ($AR = 0$).

The Shah-London correlation was validated in previous works on narrow rectangular channels [27, 34]. In the current work, it is further tested against 6 isothermal experiments from the SULTAN-JHR database, where the flow is laminar. The results are in good agreement with the experimental points (Figure 3.13).

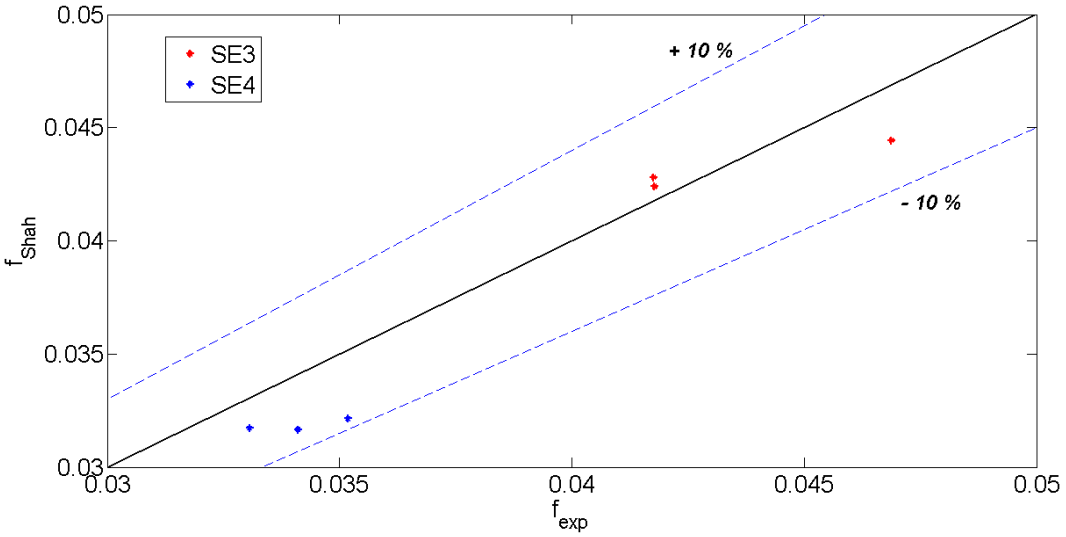

Figure 3.13: Comparison of the experimental laminar friction factor with the Shah-London correlation.

Thus, this relationship is selected for the JHR modeling. In order to simplify the modeling and the implementation in CATHARE, Eqn. (3.33) becomes:

$$f_{iso,lam} = \frac{22.69}{Re} \tag{3.34}$$

This expression is computed with an aspect ratio equal to 0.043, which is the average aspect ratio of the JHR core channel with the most unfavorable conditions, i.e. the so-called hot channel discussed in Section 6.1.

3.4.2 Single-phase laminar heat transfer

For the modeling of the fully-developed laminar single-phase heat transfer in rectangular channels, the Marco and Han correlation [35] is usually suggested (e.g. [27, 34, 36]).

It reads as:

$$Nu_{lam,FC} = 8.235\ f(AR) = 8.235\ (1 - 2.0421AR + 3.0853AR^2 + \\ - 2.4765AR^3 + 1.0578AR^4 - 0.1861AR^5) \tag{3.35}$$

where 8.235 is the Nusselt number in the case of two infinite vertical plates.

Analogously to the laminar friction factor, a simplified version of Eqn. (3.35) is implemented in CATHARE:

$$Nu_{lam,FC} = 7.56 \tag{3.36}$$

No SULTAN-JHR experiments can be used for the assessment of the correlation.

3.4.3 Laminar-turbulent transition

A flow can evolve from laminar to turbulent when a critical Reynolds number is exceeded. The process is gradual and a transition zone is observed between the two flow regimes. The lower and upper limit of the region are usually defined in terms of Reynolds number (in this thesis they are labeled as '$Re_{lim,1}$' and '$Re_{lim,2}$', respectively).

In CATHARE, the laminar-turbulent transition is not modeled. In fact, the friction and the heat transfer are determined according to Eqn. (3.1) and (3.3). As a result of this, the correlations for turbulent flows are used over almost the entire range of Reynolds numbers and the Nusselt number is over-predicted in the laminar and transition region (Figure 3.14).

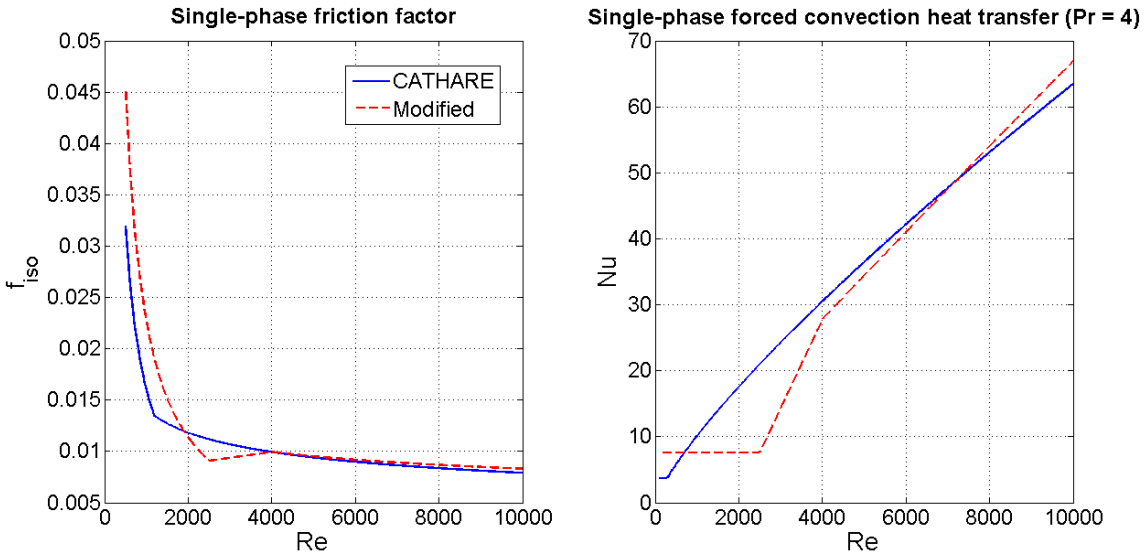

Figure 3.14: Comparison between the standard CATHARE (no laminar-turbulent transition) and the modified one.

Therefore a transition zone is introduced in the code for Reynolds numbers between 2500 and 4000, as also discussed in [17]. The friction factor and the heat transfer coefficient are given in this region by a linear combination of the laminar and turbulent correlations. This kind of approach is chosen because it is simple to be implemented and it guarantees the continuity of the scheme. Moreover, no reliable and well-established models of the laminar-turbulent transition are available for rectangular channels, and experiments to support more sophisticated solutions are scarce.

Chapter 4

Assessment of criteria for Onset of Flow Instability

The onset of flow instability can be a limiting phenomenon for the operations of thermal-hydraulic systems with parallel channels. Therefore, there has been an interest in developing design criteria that can identify OFI conditions. In the current research, a database is created by collecting experiments in narrow channels, from the literature and from the SULTAN-JHR campaign (Section 4.1). The database is used to assess selected OFI criteria (Section 4.2). The results and the optimization of some of them are discussed in Section 4.3 and 4.4. The chapter is a summary of Paper III.

4.1 Experimental database

The assessment of the OFI criteria is based on experiments in heated vertical narrow rectangular channels with relatively large width-to-gap ratios (see Figure 3.1). The tests are summarized in Table 4.1, where the main geometric features are also reported.

Table 4.1: Experimental database for OFI assessment.

Experiments	**N. tests**	**Gap [mm]**	$\mathbf{l_{heat}}$ **[mm]**	$\mathbf{L_{heat}}$ **[mm]**	$\mathbf{D_{hydr}}$ **[mm]**	$\frac{\mathbf{L_{heat}}}{\mathbf{D_{heat}}}$
Experiments with uniform heat flux						
THTL [8]	25	1.27	13.4	507.0	2.37	195.6
Casimir SE1 [37]	11	1.80	37.9	599.0	3.44	166.1
Casimir SE2 [38]	15	3.60	37.5	600.0	6.58	82.3
Casimir SE3 [39]	4	3.60	37.5	900.0	6.58	123.5
Vernier [40, 41]	26	2.00	37.0	600.0	3.80	146.1
Whittle-Forgan SE1 [7]	16	3.23	25.4	609.6	5.72	94.5
Whittle-Forgan SE2 [7]	16	2.44	25.4	406.4	4.45	83.3
Whittle-Forgan SE3 [7]	15	2.03	25.4	406.4	3.76	100.0
Whittle-Forgan SE4 [7]	12	1.40	25.4	533.4	2.65	190.9
SULTAN-JHR SE4	7	2.16	51.1	609.7	4.15	138.9
SULTAN-JHR SE3	4	1.51	51.1	609.8	2.93	196.8
Experiments with non-uniform heat flux						
Casimir NU [42]	6	3.60	37.5	517	6.58	70.9
SULTAN-JHR NU	9	1.54	49.7	599.8	2.99	186.5

The experiments are performed with an upward flow of degassed and demineralized water, and cover the following range of conditions: the outlet pressure is between 0.12 and 1.73 MPa; the heat flux between 0.4 and 14.9 MW/m^2; the mass flux between 740 and 20325 kg/m^2/s; and the outlet sub-cooling between 4.8 and 31.2 °C. In all the tests, the OFI point is determined by reducing the mass flow rate until a minimum pressure drop is reached, according to the procedure described in Section 3.2.3.

In reactor applications, dissolved gases may appear in the flow because of the radiation field and the heat flux is not constant along the core channels. Thus, the Casimir and SULTAN-JHR experimental programs also included tests with dissolved gases and with non-uniform axial heat flux profiles.

As regards the presence of dissolved gases, 2 air-saturated flow redistribution curves in Casimir SE3 [43] and 6 nitrogen-saturated in SULTAN-JHR SE4 are available. No impact of the dissolved gases was observed on the onset of flow instability, so no specific analysis is necessary. In Figure 4.1, examples from both the Casimir and SULTAN-JHR databases are given. The comparison between experiments with and without dissolved gases at the same system conditions, shows in fact a similar minimum of the curve pressure drop - mass flow rate.

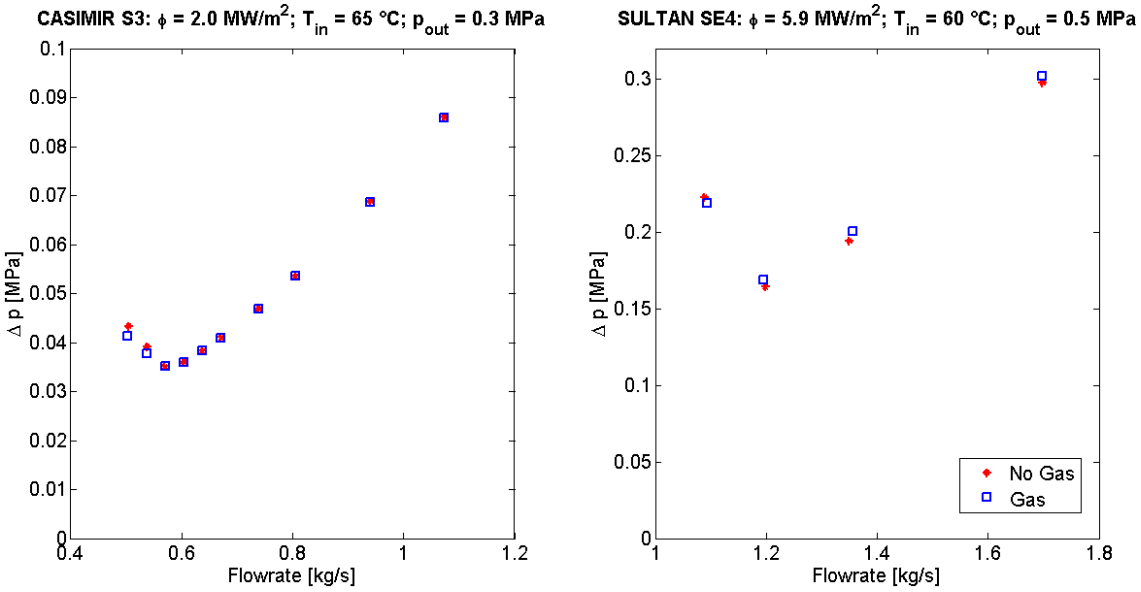

Figure 4.1: Influence of the dissolved gases in two tests with uniform heat flux.

On the contrary, the axial shape of the heat flux can affect OFI. Hence, the Casimir and the SULTAN-JHR non-uniform (NU) experiments are included in the assessment. The Casimir NU tests were performed with either decreasing or increasing heat flux profiles, and the local-to-average heat flux ratios vary approximately linearly between 0.833 and 1.214 (see Figure 3 in Paper III). The SULTAN-JHR NU experiments are described in Section 3.2.1. The system conditions are: the heat flux varies between 2.0 and 7.7 MW/m^2; the outlet pressure between 0.3 and 0.88 MPa; the mass flux between 845 and 11220 kg/m^2/s; and the outlet sub-cooling between 8.6 and 35.1 °C.

4.2 OFI criteria

The most significant OFI criteria that are studied in the work are briefly introduced. They are based on: the onset of nucleate boiling, the onset of fully developed boiling, the net vapor generation, and a global approach.

4.2.1 Criteria based on ONB and FDB

One kind of OFI criterion can be derived from the assumption that the flow instability starts, when either ONB or FDB occurs in the heated channel. The first case is based on the fact that the ONB is a prerequisite for the formation of vapor bubbles and so for the onset of flow instability, as discussed in Section 2.2. In the second case, the FDB and NVG points are supposed to occur simultaneously, which is a reasonable approximation at high pressure [44]. For instance, a FDB-based approach was used in one analysis of the JHR [45]. The general formulation of the criterion is such that the wet wall temperature is compared to the ONB or the FDB temperature, and it can be expressed as:

$$M_{Tw} = T_{sat} + \Delta T_{sat} - T_w \leq 0 \tag{4.1}$$

The wall superheat ΔT_{sat} can be estimated with the Bergles-Rohsenow ONB relationship [46]:

$$\Delta T_{sat,ONB} = 0.556 \left[\frac{\phi}{1082 \left(\frac{p}{10^5}\right)^{1.156}} \right]^{0.463\left(\frac{p}{10^5}\right)^{0.0234}} \tag{4.2}$$

Alternatively, the Forster-Greif FDB correlation can be applied, as given in Eqn. (3.28). The value of the wet wall temperature can be derived from experimental measurements or from an appropriate single-phase heat transfer correlations. In the discussion below, it is calculated with the optimized correlations described in subsection 3.3.2.1 (and labeled as 'ST-opti'). No physical meaning is associated to the negative values of M_{Tw}, since the single-phase correlation used for the wall temperature is not valid beyond ONB and FDB.

4.2.2 Criteria based on NVG correlations

Since the net vapor generation condition slightly precedes the flow excursion (see Section 2.2), NVG correlations have been extensively employed to develop OFI criteria. Examples are the Saha-Zuber and the Saha-Zuber KIT correlations.

The Saha-Zuber relationship [18] relies on theoretical considerations complemented with experimental data from test sections with several types of geometries (annular, circular and rectangular) and coolants (water and Freon) at pressure between 0.1 and 13.8 MPa. It can be written in terms of liquid enthalpy as:

$$\Delta i_{sub,NVG} = \begin{cases} \frac{\phi \ c_{p,l} \ D_{hydr}}{455 \ k_l} & \text{if } Pe < Pe_0 \\ \frac{\phi}{65 \cdot 10^{-4} \ G} & \text{if } Pe \geq Pe_0 \end{cases} \tag{4.3}$$

The Saha-Zuber KIT relationship is a modification of the above equation and is given in Eqn. (3.13). This is the standard model in CATHARE.

In this context, an OFI criterion can be built as the ratio between the local liquid sub-cooling and the one necessary to attain NVG conditions:

$$NVGR = \frac{i_{l,sat} - i_l}{\Delta i_{sub,NVG}} \tag{4.4}$$

where the denominator is calculated either with Eqn. (4.3) or (3.13). The Net Vapor Generation Ratio (NVGR) is evaluated along the channel: if the minimum value is smaller or equal to unity, then the condition for NVG and therefore for OFI, is verified. In case of uniform heat flux, the minimum always occurs at the outlet of the test section. Only the local liquid properties and the boundary conditions are needed for this kind of criterion. Thus, its application is easier than the ones based on ONB and FDB, which require an accurate knowledge of the wall temperature both in single- and two-phase flow.

4.2.3 Criteria based on global parameters

Some criteria only require the knowledge of 'global' parameters, such as the inlet and outlet flow conditions together with the geometric characteristics of the channel. The Whittle-Forgan [7] and Stelling [47] criteria fall into this category.

The Whittle-Forgan formula was developed from experiments with sub-cooled water flow and uniform heat flux, at low pressure, in four narrow rectangular channels (see Table 4.1) and in a circular tube. The experimental minima of the flow redistribution curves were correlated using the ratio:

$$R = \frac{T_{l,out} - T_{l,in}}{T_{sat,out} - T_{l,in}} \tag{4.5}$$

where the increase of liquid temperature between the inlet and outlet of the channel is divided by the temperature rise needed to reach saturation at the exit. Based on the assumption that the bubble detachment takes place at OFI and that the specific heat capacity is constant, Eqn. (4.5) was expressed as a function of the characteristic heated lengths of the channel:

$$R_{WF} = \frac{1}{1 + \eta \frac{D_{heat}}{L_{heat}}} \tag{4.6}$$

The experiments showed that the ratio R is approximately constant at OFI for a given geometric configuration. The parameter η was then derived from a best-fitting, and it is equal to 25. However, the value of 32.5 is usually suggested in the literature, because it is supposed to be conservative [48, 49]. The latter value was therefore used as reference in the current calculations.

A Flow Instability Ratio (FIR) can then be defined as [48]:

$$FIR = \frac{R_{WF}}{R} \tag{4.7}$$

where R is determined by the actual temperature rise along the channel. If the ratio is smaller than or equal to 1, the conditions for the onset of flow instability are reached.

Stelling et al. [47] developed a similar criterion using experimental data for downward water flow in vertical uniformly heated tubes with diameters between 9.1 and 28 mm. It reads as:

$$R_{Stelling} = \frac{1}{1 + \frac{0.25}{St_{SZ}} \frac{D_{heat}}{L_{heat}}} \tag{4.8}$$

In Eqn. (4.8), the quantity $0.25/St_{SZ}$ replaces the parameter η, and the Stanton number is derived from the Saha-Zuber relationship (i.e. $St_{SZ} = 0.0065$). The formula was validated against experiments with $Pe > Pe_0$.

In addition, an alternative version of the Stelling criterion is investigated. This is obtained by estimating the Stanton number with the Saha-Zuber KIT correlation (3.13). As a result, Eqn. (4.8) can be re-written as:

$$R_{Stelling,SZ-KIT} = \begin{cases} \frac{1}{1+\frac{5}{4 \cdot 455}\left(\frac{D_{heat}}{L_{heat}}\right)Pe} & \text{if } Pe < 0.52Pe_0 \\ \frac{1}{1+\frac{2}{4 \cdot 455}\left(\frac{D_{heat}}{L_{heat}}\right)Pe\left(\frac{Pe}{Pe_0}\right)^{-1.4}} & \text{if } Pe \geq 0.52Pe_0 \end{cases} \tag{4.9}$$

In this case, the FIR is also dependent on the Peclet number at the outlet of the test section.

4.3 Results with uniform heat flux

The outcomes from the application of the different OFI criteria to the experiments with uniform heat flux, are discussed. Then, the optimization of the most attractive criteria is presented.

4.3.1 Comparison with the selected OFI criteria

The results of the assessment are summarized in Table 4.2. The mean value is a measure of how close a criterion is to its optimal value on average. The standard deviation provides the variability of the criterion to the flow conditions and the experimental set-ups: a smaller spread of the results indicates that the performance is less sensitive to the differences in the experiments.

Table 4.2: Tests with degassed water and uniform heat flux: summary of results.

	mean	**std**	**min**	**max**
Criteria based on ONB and FDB				
M_{Tw-ONB} (ST-opti) [°C]	-26.07	13.13	-74.50	-1.33
M_{Tw-FDB} (ST-opti) [°C]	-13.02	12.7	-62.7	10.0
Criteria based on NVG correlations				
NVGR Saha-Zuber	0.792	0.244	0.476	2.615
NVGR Saha-Zuber KIT	0.504	0.174	0.225	0.998
Criteria based on global parameters				
FIR Whittle-Forgan (η = 32.5)	0.967	0.040	0.888	1.064
FIR Stelling	0.932	0.046	0.845	1.037
FIR Stelling (Saha-Zuber KIT)	0.825	0.088	0.644	1.000

The criterion based on the ONB leads to relatively large negative values, so OFI is always identified in a fairly conservative manner. Such an outcome has to be expected because the ONB is an OFI prerequisite, as previously discussed.

The approach using the Foster-Greif FDB correlation provides negative values in most of the cases. However, OFI is not predicted in the SULTAN-JHR SE3 and some of the Whittle-Forgan SE4 experiments (see details in Paper III).

When applying the NVG criteria, the conditions for flow instability correspond to NVGR values that are less than 1. The Saha-Zuber relationship predicts OFI in most of the tests, but there are issues with the THTL, Whittle-Forgan and SULTAN-JHR tests at $Pe < Pe_0$ (see Figure 4.2). In view of this, the transition between the thermally and hydro-dynamically driven bubble detachment in narrow channels seems to occur for a Peclet number that is below $Pe_0 = 70000$. Such a behavior was already observed in previous works [50].

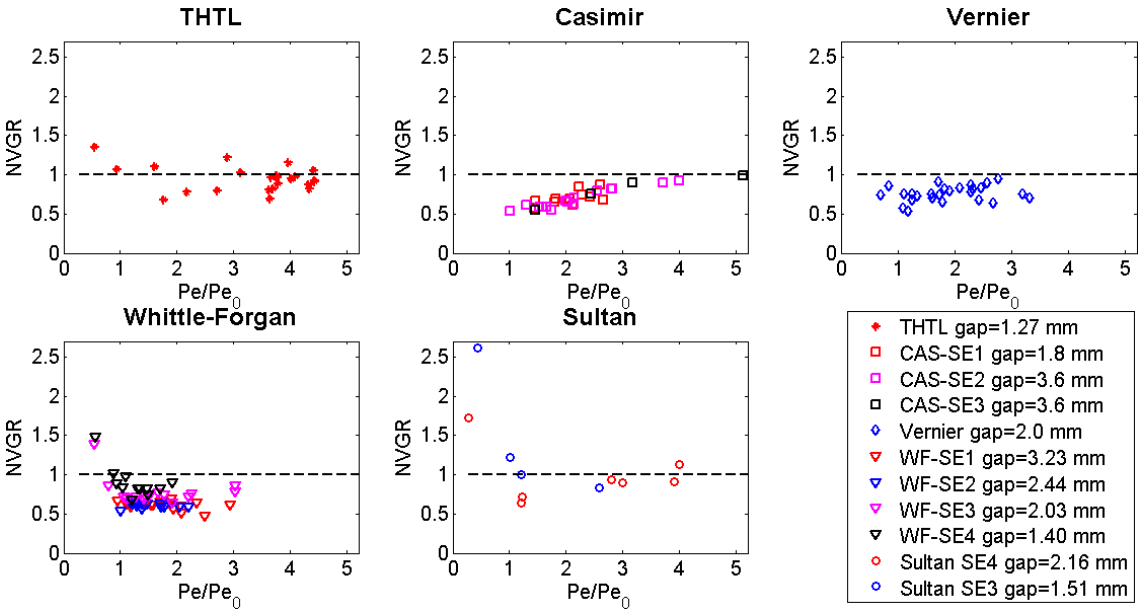

Figure 4.2: NVGR with Saha-Zuber correlation (4.3).

On the other hand, the Saha-Zuber KIT correlation is found to be conservative, since the NVGR is always smaller than 1. In Figure 4.3 a clear trend can also be recognized, where the NVGR approaches unity with the increase of Pe. This suggests that the OFI and the NVG phenomena tend to be closer at high Peclet. In contrast to the standard Saha-Zuber correlation, good results are obtained at low Pe, maybe due to the smaller transition value equal to $0.52 \cdot Pe_0$.

The Whittle-Forgan and the Stelling FIR perform in a similar manner, with a tendency to predict conservatively the flow redistribution. In both cases the estimated mean value is below 1 and the standard deviation is relatively narrow. Nevertheless, the Whittle-Forgan formula exceeds 1 for channels with small gaps (i.e., the THTL, Whittle-Forgan SE4, and SULTAN-JHR SE3) and for high values of the Peclet number (see Casimir and SULTAN-JHR SE4), as shown in Figure 4.4. The Stelling relationship can capture more points, since it computes smaller values using a higher η, but OFI

is still not identified in some tests.

The FIR based on the Saha-Zuber KIT correlation can predict the OFI occurrence in all the experiments, consistently with the NVRG built on the same correlation. The standard deviation is larger than the ones for the other FIR criteria, though.

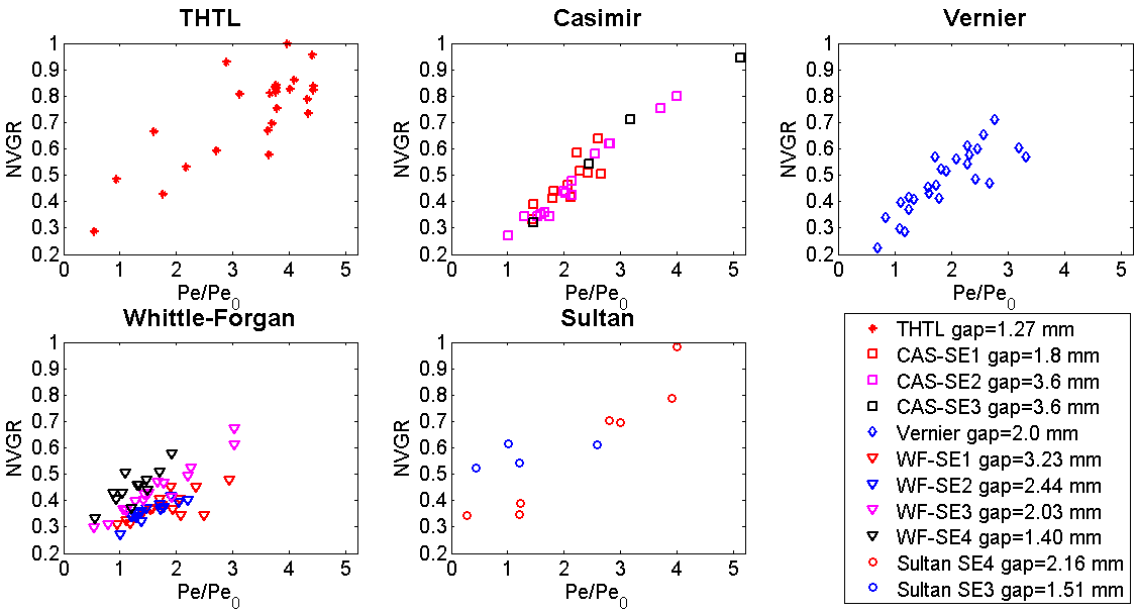

Figure 4.3: NVGR with Saha-Zuber KIT model (3.13).

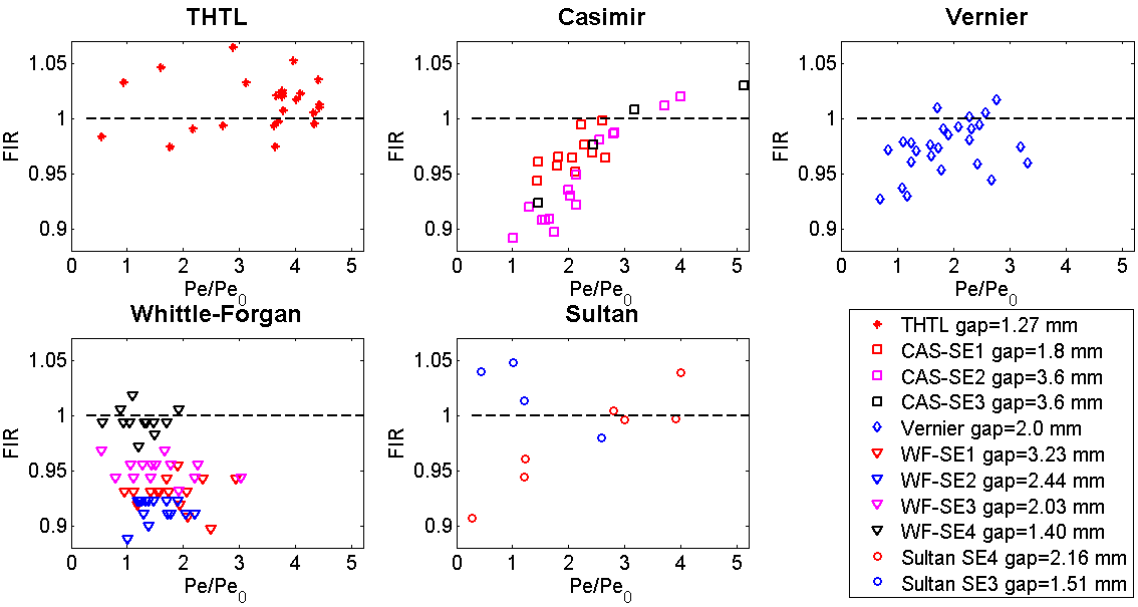

Figure 4.4: Whittle-Forgan FIR ($\eta = 32.5$).

4.3.2 Development of optimized criteria

As mentioned above, the FIRs only require global parameters, so they are particularly attractive for application purposes. The OFI condition corresponds to a ratio equal to

1 in the ideal case, or less than 1. In order to have results closer to the ideal value 1 with a smaller spread, the FIRs are optimized over the available data. Two criteria are then developed: one is based on the Whittle-Forgan correlation; and one is based on the Saha-Zuber KIT correlation. This section is focused on the second option, while the complete discussion is available in Paper III.

A best-fitting of the experimental data can be used to adjust the constants of the Saha-Zuber KIT relationship. For this purpose, Eqn. (3.13) may be re-written as:

$$Y = a_Y \left(\frac{Pe}{Pe_0} \right)^{b_Y} \tag{4.10}$$

The quantity Y can be estimated from the experiments as:

$$Y = \frac{\Delta i_{sub}}{\left(\frac{\phi c_{p,l} D_{hydr}}{65 \cdot 10^{-4} k_l Pe_0} \right)} \tag{4.11}$$

A linear regression fits quite accurately the experimental results with a coefficient of determination R^2 equal to 0.85, and the values of the constants a_Y and b_Y are equal to 0.6733 and -0.8448 respectively.

The comparison between the Saha-Zuber KIT correlation and the best-fitting model with respect to the experimental points, is shown in Figure 4.5.

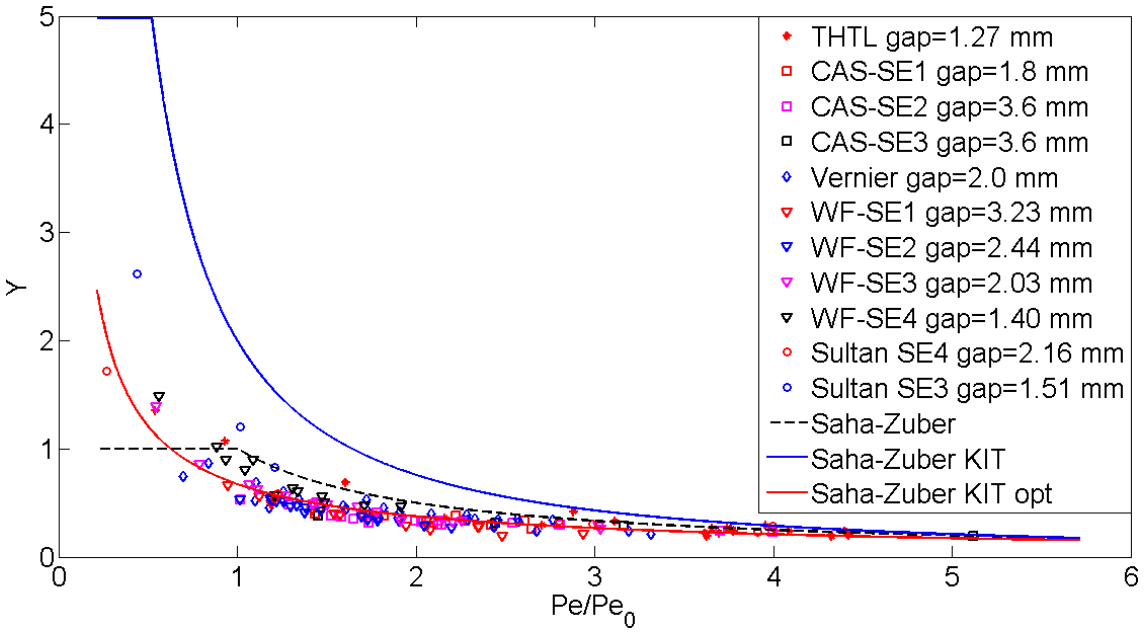

Figure 4.5: Y parameter as a function of Pe/Pe_0.

The Saha-Zuber KIT relationship (blue curve) can be considered conservative, since the calculated values of Y are always higher than the experimental ones. Such a discrepancy increases with the decrease of the Peclet number, which may be due to the increasing delay between the NVG and the OFI. The best-fitting curve (in red) has a similar shape, but the different slope allows to better capture the behavior of the data at low Peclet. In the figure, the standard Saha-Zuber is also included. As discussed in subsection 4.2.2, this correlation underestimates the experimental points at low Peclet numbers.

Using the result of the best-fitting, the R parameter can be modified as:

$$R_{Stelling,SZ-KITopt} = \frac{1}{1 + \frac{0.6733}{4 \cdot 455} \left(\frac{D_{heat}}{L_{heat}}\right) Pe \left(\frac{Pe}{Pe_0}\right)^{-0.8448}} \tag{4.12}$$

The comparison of the optimized FIR with the experimental data is shown in Figure 4.6. The experimental points are distributed around the ideal value of 1 with a relatively small standard deviation, due to the best-fitting procedure. The performances of the criterion can be summarized as: mean value = 0.992; standard deviation = 0.032; minimum = 0.916; and maximum = 1.085. Since some points are above 1, the maximum value can be used as a conservative threshold for practical purposes.

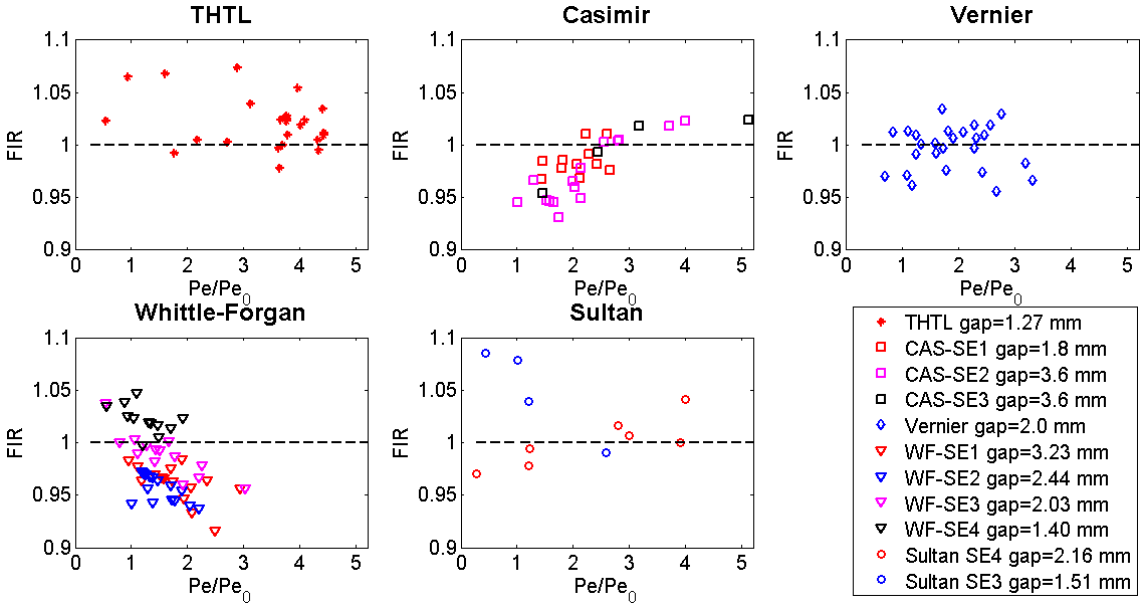

Figure 4.6: Best-fitting FIR Saha-Zuber KIT (4.12).

This optimized formula has been developed for Peclet numbers between 15,889 and 358,460. The applicability outside its range of validity would require further validation work, especially at low Peclet numbers.

4.4 Influence of the non-uniform heat flux profile

The OFI criteria were developed in conditions of uniform axial heat flux. In order to evaluate their applicability to cases where the axial heat flux is not constant, the Casimir NU and SULTAN-JHR NU experiments are also analyzed.

In Figure 4.7, a comparison is reported between two Casimir NU tests with an increasing and a decreasing axial heat flux respectively. The flow conditions are similar, but the minimum of the flow redistribution curve occurs at a higher mass flow rate for the increasing axial heat flux.

The global performances of the OFI criteria when applied to these experiments, are comparable to the ones found in the case with uniform heat flux (see details in Paper III). Still, an effect due to the kind of heat flux profile can be seen. The OFI criteria can be more conservative with a heat flux at the exit of the channel smaller than the

average one, similarly to the SULTAN-JHR NU experiments. On the contrary, the reliability of the predictions may be reduced for higher heat fluxes at the outlet, as in the Casimir NU tests with increasing axial power profiles. Such an observation is mainly valid for the integral criteria (FIRs), while the criteria that rely on the local flow conditions (e.g., NVGR), can take to some extent the variation of the heat flux into account. For other types of arrangements in terms of heat flux profile, further analyses would be required.

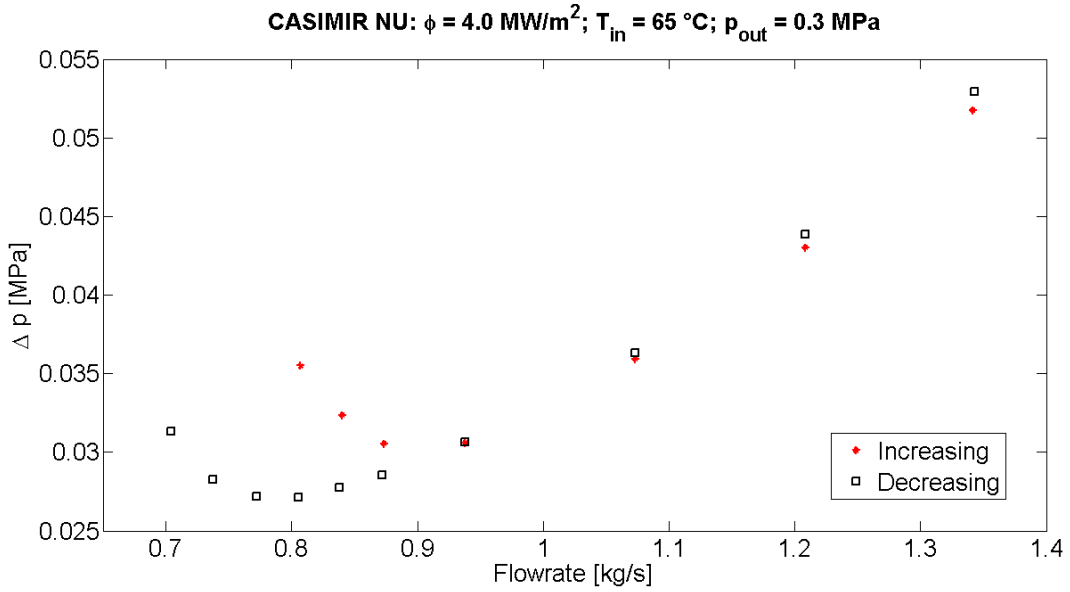

Figure 4.7: Flow redistribution curves with non-uniform heat flux (Casimir NU).

Chapter 5

Best-estimate plus uncertainty methods for safety analysis

The work discussed in Chapter 3 and 4 is related to the evaluation and optimization of the thermal-hydraulic modeling of the JHR. The next step is to use these outcomes in combination with a best-estimate plus uncertainty approach to perform the safety analysis of the JHR (Paper IV and Chapter 6). The current chapter is then an introduction to the best-estimate plus uncertainty methodology applied in this research. The general background is provided in Section 5.1. The best-estimate approach combined with conservative assumptions or with an uncertainty evaluation is discussed in Section 5.2. The statistical methodology for uncertainty propagation, developed at GRS, is illustrated in Section 5.3. The sensitivity measures for determining the most influential sources of uncertainty are reported in Section 5.4. Finally, the uncertainty and sensitivity platform URANIE is introduced in Section 5.5.

5.1 Background

The safety objective in nuclear reactors is to preserve the integrity of the barriers against the release of radioactivity. For this reason, sufficient margins should exist between the operational values of the reactor parameters and the limiting values over which damage to the barriers can occur. The principle is schematized in Figure 5.1.

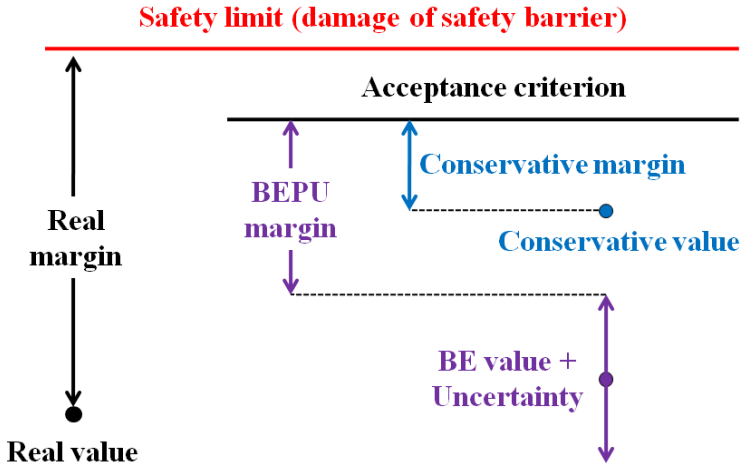

Figure 5.1: Safety margins in a nuclear power plant.

In practical applications, both the real value and the safety limit are not known precisely. Thus, the safety margin is usually defined as the difference (or ratio) between a threshold value set up by the regulatory body (i.e., acceptance criterion) and the calculated value. Key parameters for safety such as the peak cladding temperature in the fuel elements, can be determined under nominal and accidental conditions using CATHARE, TRACE, or other similar codes. These Best-Estimate (BE) system codes allow to analyze the thermal-hydraulic behavior of a NPP according to the state-of-the-art knowledge in the field.

5.2 Best-estimate plus uncertainty approach

Best-Estimate codes in combination with pessimistic hypotheses for the input parameters have been extensively employed for the safety analysis of nuclear reactors. As shown in figure 5.1, the calculated 'conservative' value is expected to be closer to the acceptance criterion than the real value or a realistic prediction. The relative safety margin is denoted as 'conservative'. Due to the degree of conservatism, this kind of analysis can lead to unreasonable results and even mask important safety issues. Therefore, in the past few decades, there has been an increasing interest in the use of BE codes with realistic assumptions, complemented with an uncertainty analysis (i.e. BEPU, Best Estimate Plus Uncertainty) [51]. In this approach, the evaluation of the impact of the uncertainties is crucial because of the less penalizing character of the simulations. Then, the BEPU methodology provides a BE value of the parameter within an uncertainty band. The upper (or lower) limit of the uncertainty band is used to quantify the safety margin with respect to the acceptance criterion.

A historical milestone for the diffusion of BEPU is the US Code of Federal Regulation 10 CFR 50.46 [52] issued in 1988, which allowed the use of this approach in the licensing and safety assessment process beside traditional conservative models. From that moment, several methodologies for uncertainty analysis have been developed. The methodologies based on the 'extrapolation of output uncertainties', like the CIAU [53], extracts the error on the calculated results from suitable experiments in Integral Test Facilities (ITF) and real plant data. On the other hand, the 'propagation of input uncertainties' (e.g., CSAU [54] and GRS [55]) require the identification and quantification of the uncertainties related to the relevant input parameters. The output uncertainties can then be obtained performing several simulations by varying input quantities. Furthermore, the results of the uncertainty propagation can be used for a sensitivity analysis to identify the most influential parameters.

5.3 The GRS methodology

In the current research, the GRS methodology is employed. It was developed at Gesselschaft für Angalen und Reaktorsicherheit (GRS) in Germany, and it is based on a statistical propagation of selected input uncertainties throughout the simulations, so that uncertainty bands for the results can be determined with a certain probability and degree of confidence. The different steps are illustrated in Figure 5.2, and briefly described in the following subsections.

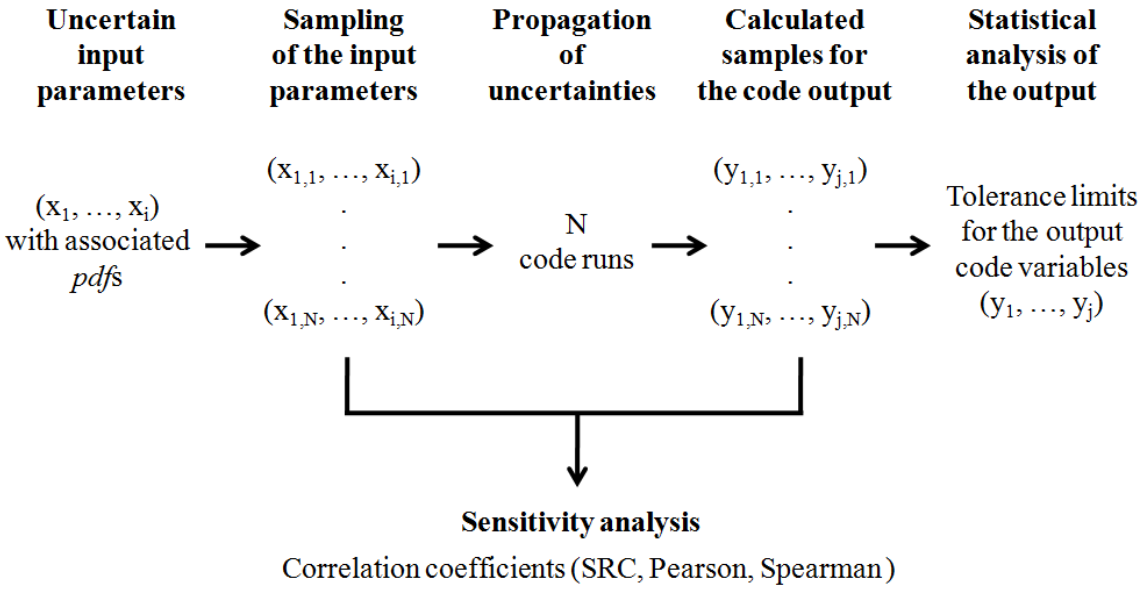

Figure 5.2: Schematic description of the GRS methodology.

5.3.1 Identification and quantification of input uncertainties

The first step in the GRS methodology is to identify the possible sources of uncertainty connected to the system and scenario under study.

It is possible to distinguish two main categories of uncertainty [56]: Aleatory (or Irreducible) and Epistemic (or Reducible). The aleatory uncertainties are related to the stochastic variations of the physical system or the environment, while the epistemic uncertainties are due to the lack or limitation of knowledge.

Depending on the application, several sources of uncertainty (either aleatory or epistemic) can be identified. In a BE thermal-hydraulic simulation of a nuclear power plant, five main sources [51] can be considered:

- *Code and Model uncertainties*, mainly associated to the numerical schemes and the physical models of the code;
- *Plant uncertainties*, related to the initial and boundary conditions, and to the geometry and material data of the system;
- *Representation uncertainties*, due to the discretization (or nodalization) of the system;
- *Scaling uncertainties*, arising from the application of correlations based on scaled experiments, to full scale systems;
- *Users' effects*, introduced by the individual modeling choices of the users.

The representation, scaling and user effect uncertainties are difficult to determine and quantify, so they are often neglected.

Once the relevant input uncertainties are identified, they need to be quantified in terms of probability distribution functions (*pdf*s). The determination of the *pdf*s relies on different data, such as specifications from the manufacturers, appropriate SET experiments, plant design data and the literature. In particular, when SETs are available, the accuracy of a thermal-hydraulic correlation can be evaluated by comparing the experimental measurements to the simulation of these tests, as described in Paper I. If such data are not sufficient or available, then conservative assumptions/judgments may be used. In this case, an uniform distribution for the *pdf* is usually chosen, so that no value is privileged [55].

5.3.2 Propagation of input uncertainties

For each of the uncertain input parameters, a sample of size N is generated from the associated *pdf*, using a Simple Random Sampling (SRS) technique. Then, all the uncertain inputs are changed simultaneously according to the values of the random samples, and a calculation is performed for each set of variations. As a result, samples of size N are obtained for the code output variables and output uncertainty bands can be quantified, for instance, in terms of tolerance intervals.

The number of code calculations N depends on the requirements for the tolerance limits. A tolerance interval is defined as an interval that includes at least a portion q of the population under study, with a confidence level γ. The limits of a tolerance interval can be estimated by a sample of the population, whose size N is related to q and γ. For one-sided tolerance limits, given q and γ, N can be determined by using the Wilks formula [57]:

$$\gamma \geq 1 - q^N \tag{5.1}$$

An extension of the Wilks formula can be written as [58, 59]:

$$\gamma \geq 1 - \sum_{s=0}^{r+m-1} \binom{N}{s} (1-q)^s \, q^{N-s} \tag{5.2}$$

This expression allows to estimate N in such a way that at least a portion q of the population lies between the r^{th} smallest and the m^{th} largest value of the sample, with a confidence level γ. The one-sided tolerance limit with respect to different q and γ, corresponds to the condition $r+m=1$, and Eqn. (5.2) then reduces to Eqn. (5.1). In the case that q and γ are fixed and $r+m>1$ is used, then the upper (lower) one-sided tolerance limit can still be evaluated by neglecting the $(r+m-1)$ largest (smallest) values and taking the $(r+m)^{\text{th}}$ maximum (minimum). The minimum number of code runs necessary for different combination of parameters is shown in Table 5.1.

For the purpose of nuclear safety, the regulation authorities commonly accept analyses with q and γ equal to 0.95. This corresponds to a minimum of 59 calculations for one-sided tolerance intervals (according to Table 5.1). Nevertheless, the use of more code runs allows a more reliable and precise estimation of the tolerance limits, and it improves the sensitivity analysis [60].

Table 5.1: Minimum number of code runs, according to Eqn. (5.2).

$\mathbf{r+m}$	$\mathbf{q=\gamma=0.95}$	$\mathbf{q=0.95;\gamma=0.99}$	$\mathbf{q=0.99;\gamma=0.95}$	$\mathbf{q=\gamma=0.99}$
1	59	90	299	459
2	93	130	473	662
3	124	165	628	838
4	153	198	773	1001
5	181	229	913	1157
6	208	259	1049	1307
7	234	288	1182	1453
8	260	316	1312	1596
9	286	344	1441	1736
10	311	371	1568	1874
11	336	398	1693	2010

5.4 Sensitivity analysis

The input and output samples obtained from the uncertainty analysis are used to perform a sensitivity analysis. The goal is to assess the impact of the input parameters on the calculated outputs, to better understand the phenomena/models involved in the scenario, and to identify which improvements of the modeling are most needed.

In this work, the possible correlation between inputs and outputs of the code are evaluated with: the Pearson correlation coefficient, the Spearman correlation coefficient, and the Standardized Regression Coefficient (SRC). These sensitivity measures can vary between -1 and +1. When the value is positive, the output increases as the input quantity increases, and vice versa. No correlation is expected in case of a zero value; while a value of -1 or +1 indicates a very strong relationship.

The Pearson correlation coefficient quantifies the strength of the linear relationship between two samples. It is expressed as the ratio between the covariance of the two samples and the product of their standard deviations [61]. For a code output y and a generic input parameter x_i, the coefficient can be determined as:

$$c_{Pearson,i} = \frac{\sum_{k=1}^{N} \left(x_{i,k} - \bar{x}_i\right)\left(y_k - \bar{y}\right)}{\left(\sum_{k=1}^{N} \left(x_{i,k} - \bar{x}_i\right)^2 \sum_{k=1}^{N} \left(y_k - \bar{y}\right)^2\right)^{1/2}} \tag{5.3}$$

where $x_{i,k}$ and y_k are the k^{th} elements of the two samples; and $\bar{x}_i$ and $\bar{y}$ are the mean values.

The Spearman rank correlation coefficient is based on a non-parametric approach, which treats the sample values in terms of their ordered ranks (indicated as r_y and r_{x_i}). No linear assumption is therefore needed and the coefficient measures how strongly monotonic the relationship between the two variables is [61]. Analogously to the Pearson coefficient, the ratio between the covariance of the ranked samples and the product of the standard deviations is used:

$$c_{Spearman,i} = \frac{cov\left(r_y, r_{x_i}\right)}{std\left(r_y\right) std\left(r_{x_i}\right)} \tag{5.4}$$

The SRC is based on a multi-linear regression of the code output y as a function of the different input variables x_i [61]:

$$y = \xi_0 + \sum_{i=1}^{N_I} \xi_i x_i \tag{5.5}$$

where N_I is the number of input variables. Using the samples for the output y and the input parameters x_i from the uncertainty analysis, a set of linear equations can be written and the regression coefficients ξ_i can be computed with a least square method. To remove the influence of the units of measurement, they are normalized as:

$$SRC_i = \xi_i \frac{std(x_i)}{std(y)} \tag{5.6}$$

The correlation coefficients are meaningful only if their absolute values are greater than a critical value. The latter is calculated from the Student's t distribution and depends on the sample size and the significance level (i.e. the probability of rejecting a true hypothesis that two parameters are not correlated). In fact higher sample sizes or significance levels lead to smaller critical values. Tables for the critical value can be found in statistics books, e.g. [62].

5.5 Uncertainty and sensitivity platform URANIE

For the application discussed in Paper IV and Chapter 6, the 'Uncertainty and Sensitivity' platform URANIE is employed. This software [63] was created at CEA and is based on the data analysis framework ROOT [64]. It has an object-oriented and modular structure with several built-in libraries for uncertainty and sensitivity analyses. The platform can be used to sample the uncertain parameters, modify the input files for the computational codes (e.g. CATHARE), launch the simulations, retrieve and analyze the output results. In addition, the CIRCE methodology used in Paper I for the evaluation of the accuracy of the thermal-hydraulic correlations in CATHARE, is embedded in URANIE.

Chapter 6

Analysis of a Station Blackout scenario in JHR

In Paper IV, the BEPU methodology is applied to the analysis of a hypothetical Station Black-Out (SBO) scenario in the Jules Horowitz Reactor. The calculations are performed with the system code CATHARE 2 (version 'v25_3 mod5.1'). For a more realistic modeling of the narrow channels in the JHR core, the code is modified according to the outcomes of Chapter 3. One of the crucial issues in the scenario is the potential for flow instabilities, therefore the investigation of the onset of flow instability relies on the recommendations given in Chapter 4.

The CATHARE nodalization of the JHR used for the calculations, is first described in Section 6.1. The nominal simulation of the scenario and the associated safety criteria are presented in Section 6.2 and 6.3. The propagation of the input uncertainties to the code results and the sensitivity analysis follow the GRS methodology and they are carried out with the platform URANIE. The main results are summarized in Section 6.4 and 6.5. This study is an alternative to the approach [45], which is based on more conservative assumptions.

6.1 CATHARE input model of the JHR

A simplified version of the primary circuit of the JHR is given in Figure 6.1. During normal operation, the reactor power is removed by 3 redundant loops equipped with pumps, heat exchangers (connected to the secondary circuit) and a pressurization line (not shown in Figure 6.1). Several safety systems are implemented to deal with possible accidents:

- one supplementary pump (RPPULTIM) is available in parallel to one of the main pumps, and it runs on batteries that can supply power for, at least, 2 hours;
- 3 aspiration lines are connected to the reactor pool with non-return check-valves;
- 2 redundant RUC/RUP systems can be used for the removal of the decay heat by forced circulation.
- a natural circulation loop can be established by opening manually two valves at the entrance and outlet of the reactor core;

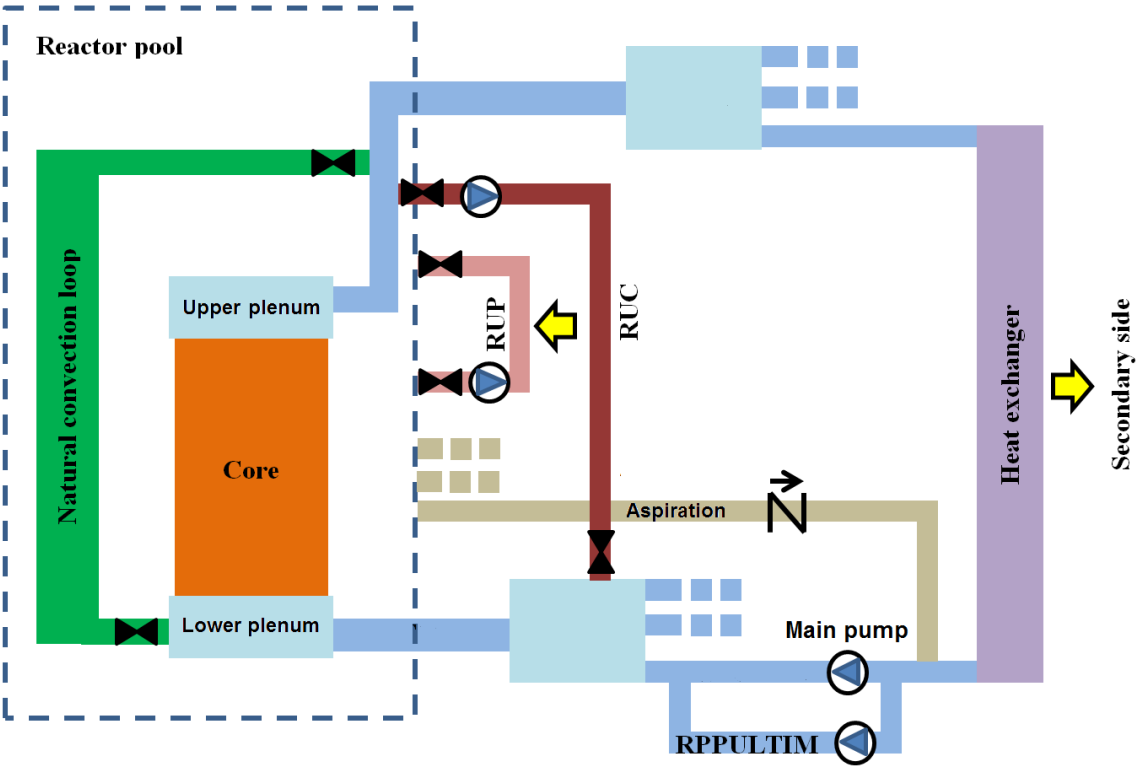

Figure 6.1: Modeling of the JHR primary circuit in CATHARE: schematic.

The CATHARE nodalization of the core is shown in Figure 6.2. The core region is enclosed between a lower and upper plena described by two 0-D volumes.

The reactor power is generated in 34 fuel assemblies, and one of them is assumed to be at higher power (the hot fuel assembly) in comparison with the other 33 (the mean fuel assemblies). Each of the mean fuel assemblies is given as a combination of: a) a 1-D module for the flow between the fuel plates; and b) a 1-D module for the flow in the central region where a control rod or an experimental device of type 1 is placed.

As depicted in Figure 6.3, the model of the hot fuel assembly consists of: a) a 1-D module for the flow in the two sectors with average power; b) a 1-D module for the flow in the sector at higher power without the hottest narrow channel; c) a 1-D module for the flow in the hottest narrow channel. A 1-D module is also added for the flow to the central region of the hot fuel assembly, where a control rod is located. The highest power in the hot channel is imposed by applying two peaking factors: $F_{element}$ is the power ratio between the hot and mean FAs (equal to 1.487), and F_{radial} is the ratio between the hot and mean channels (equal to 1.1567). A further penalization is the under-feeding of the hot channel, which is due to the geometric configuration of the FA inlet [65]. Such a phenomenon causes the mass flow rate in the hot channel to be lower than in the ideal case (based on the flow areas of the channels and isothermal conditions). The reduction was estimated with CFD calculations and it is approximately equal to 6.2% [65]. In CATHARE, the under-feeding is modeled with a localized pressure drop (nominal loss coefficient $K_{SSALIM} = 0.583$) at the entrance of the hot channel.

In addition to the fuel assemblies, 3 experimental devices of type 2, the vessel and core by-pass are modeled, and a 1-D module is used for the flow through each of them.

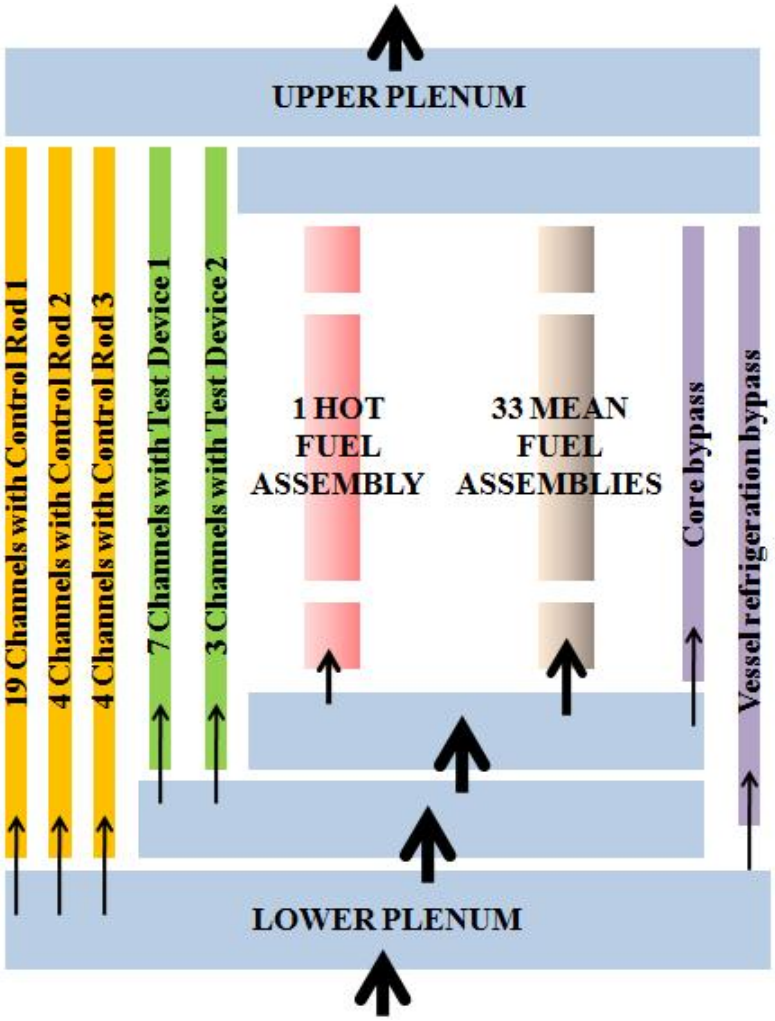

Figure 6.2: Modeling of the JHR core in CATHARE.

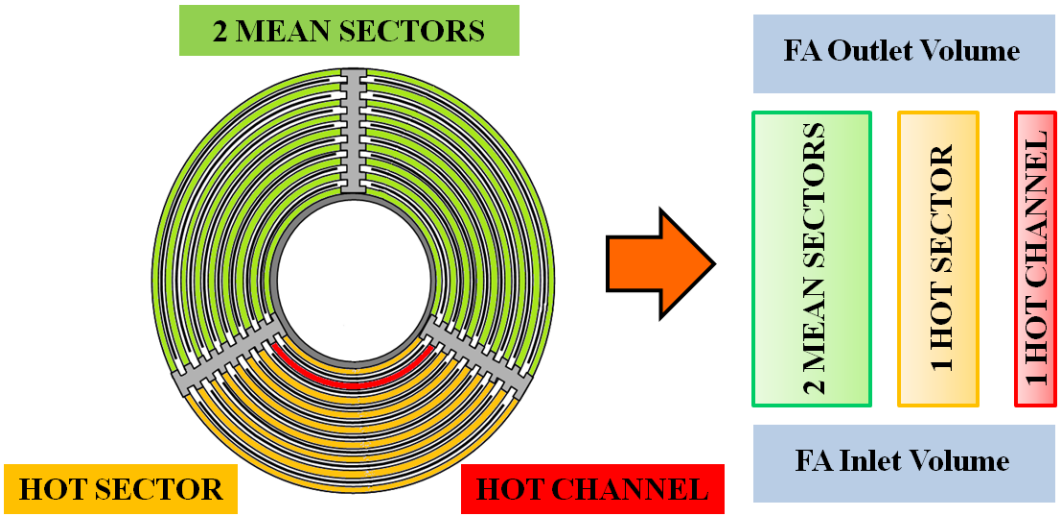

Figure 6.3: Modeling of the hot fuel assembly in CATHARE.

6.2 Simulation and description of the scenario

The station blackout leads to a loss of power supply to the systems of the nuclear reactor. In order to evaluate the JHR design in more severe conditions, two additional malfunctions are assumed: the activation of the RUC/RUP system fails; and the emergency batteries for the RPPULTIM pump run only for 1h and 20 min instead of the expected period of 2 hours. The simulated behavior of the reactor evolves as follows:

Initiation of the blackout
At t = 0 s, the blackout takes place. The progressive loss of the primary pumps and of the pressurization pump causes the decrease of the mass flow rate in the core (Figure 6.4a). The system pressure and the core pressure drop reduce consistently (Figure 6.4c and 6.4d). The temperatures in the core increase (Figure 6.4f), because the reactor power is still at the nominal value (Figure 6.4e). The fuel temperature reaches its maximum value equal to 111.9 °C.

Reactor scram
The pressure drop hits a first threshold and the reactor is automatically scrammed at t = 12.2 s (Figure 6.4d and 6.4e). The temperatures in the core decrease due to the reactor shut down.

Activation of safety systems
The pressure drop reaches a second threshold and the activation signal for the safety systems is generated at t = 21.2 s. The start-up of the RUC/RUP system fails and only the auxiliary pump RPPULTIM contributes to the circulation of the coolant. The outlet core pressure stabilizes at the value of 0.175 MPa and remains approximately constant for the rest of the simulation. The cladding temperature reaches its peak value of 110.6 °C, at t = 185 s.

Opening of natural convection valves
After 20 minutes from the activation of the safety systems (t = 1221.2 s), the natural convection valves are manually opened by the operators. The total core flow rate becomes a combination between the forced flow driven by the RPPULTIM pump and the water coming from the pool. The temperatures in the core decrease because of the higher mass flow rate.

Stop of the RPPULTIM pump
The RPPULTIM pump is assumed to stop at t = 4821.2 s. A reduction of mass flow rate occurs so that the temperatures start to rise again. The initial increase of temperature is rapidly compensated by the colder mass flow coming from the pool to the inlet of the core. The residual heat can then be removed by natural convection for the rest of the transient.

In the analysis of the scenario, the minimum liquid sub-cooling, the Reynolds and the Peclet number are also relevant parameters (see Figures 6.4i and 6.4l). The coolant remains largely sub-cooled during the whole transient, and no vapor is produced.

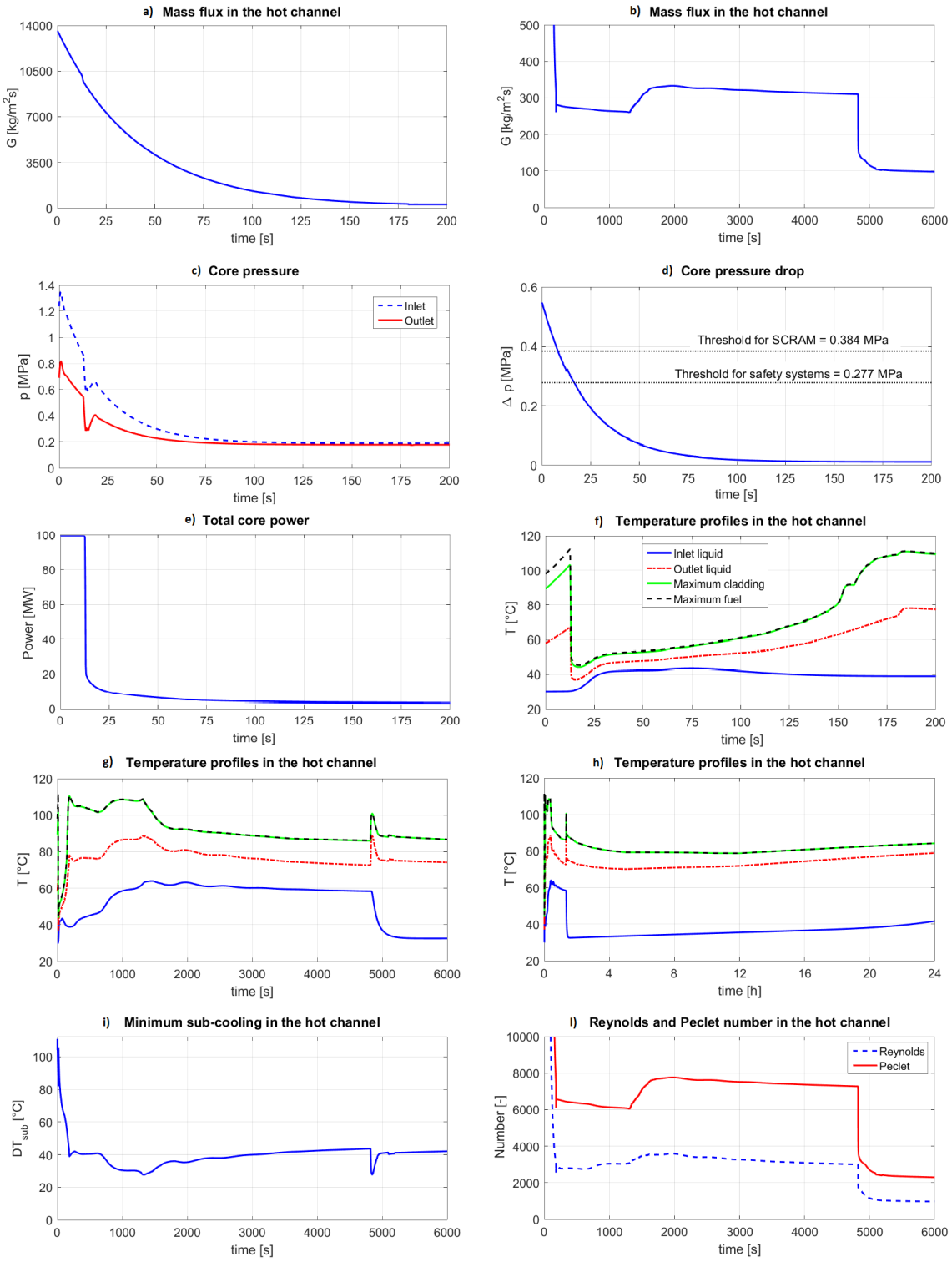

Figure 6.4: Best-estimate simulation: time evolution of relevant parameters.

The Reynolds number is used to identify the turbulent or laminar conditions of the flow. At the beginning of the transient, the reactor is cooled by turbulent forced convection, however the reduction of mass flow rate causes the Reynolds number to become small. After the first 180 seconds, the Reynolds number is between 2500 and 4000, i.e. the flow is in the laminar-turbulent transition region. When the RPPULTIM

pump stops, the Reynolds number is estimated to drop to about 1000, and the core is cooled by laminar natural convection.

A similar behavior is observed for the Peclet number, which is used for the evaluation of several OFI criteria (see Chapter 4). The Peclet number is characterized by a relatively large value under nominal conditions ($Pe = 323668$), but drops rapidly due to the reduction of the mass flow rate. A value equal to 2350 is finally reached after the RPPULTIM pump stops.

6.3 Safety criteria

The main concern for the safety of the reactor is related to the potential overheating of the core. Such an issue can indeed have dangerous consequences. The cladding can lose its integrity and radioactive material can be released from the fuel to the coolant. In addition, deformation of the fuel plates can take place, impact the geometry of the channels, and thus compromise the coolability of the reactor core. To avoid any damage, three constraints are imposed. The possible increase of the cladding temperature shall be limited before any buckling of the fuel plates can arise. The decrease of the mass flow rate shall not cause flow instabilities that can deteriorate the heat transfer in the channels (according to the mechanisms described in Section 2.2). Boiling crisis which can lead to an abrupt excursion of the cladding temperature shall be prevented. In summary, the analysis of the scenario shall demonstrate that the three safety criteria are met, namely:

- The Peak Cladding Temperature (PCT) shall be smaller than 400 °C;
- No Onset of Flow Instability shall occur;
- No Critical Heat Flux shall occur.

From the assessment study discussed in Chapter 4, the criterion based on the Saha-Zuber KIT correlation (Eqn. (3.13)) can predict the onset of flow instability in a conservative manner. Then, the related NVGR (Eqn. (4.4)) is applied in this analysis. The optimized criterion developed in Section 4.3.2 is not used for the prediction of OFI in this scenario, because the Peclet number is outside the range of validity during a large part of the simulation (see Figure 6.4l).

The CHF is evaluated with the Sudo correlation (see Section 3.3.4) and the CHFR is given according to Eqn. (3.29).

6.4 Uncertainty analysis

The GRS methodology illustrated in Section 5.3 is applied to determine the uncertainty bands for the peak cladding temperature, the minimum NVGR and the minimum CHFR, when simulating the SBO scenario.

The input uncertainties included in the analysis are reported in Table 6.1 and detailed in Paper IV. Each of the uncertain parameters is sampled with a Simple Random Sampling technique, and the size of the samples is equal to 336. The results from the 336 calculations allow to estimate the tolerance limits for the output variables,

using $r + m = 11$, given q and γ equal to 95% (see Table 5.1). Therefore, the 11^{th} largest (smallest) sample value can be used for the 95-95 upper (lower) one-sided tolerance limit, while the maximum (minimum) sample value is associated to higher q and γ. All the performed simulations were successful, so that no treatment of the failed runs was necessary.

Table 6.1: Selected input uncertainties: range and distributions.

Parameter	Nominal	Distribution	Uncertainty	Reference
Initial and boundary conditions				
Hot channel gap [mm]	1.95	Uniform	±0.31	Design data
Core power [MW]	100	Uniform	90.7 - 109.7	Design data
Peaking factor	1.487	Uniform	1.487 - 1.790	Design data
Inlet temperature [°C]	30	Uniform	29.4 - 32.1	Design data
Total core flow rate [m^3/h]	7400	Uniform	6330 - 7922.4	Design data
Outlet core pressure [MPa]	0.69	Uniform	0.65 - 0.70	Design data
Hot channel under-feeding (K_{SSALIM})	6.2% (0.583)	Uniform	4% - 8% (0.363 - 0.776)	[45, 65]
Properties of materials				
Fuel conductivity [W/mK]	55	Uniform	10 - 100	Design data
Fuel heat capacity [J/kgK]	Paper IV	Uniform	±2.5%	Design data
Cladding conductivity [W/mK]	Paper IV	Uniform	±11%	Design data
CATHARE closure laws				
Turbulent friction factor	Eqn. (3.20)	Normal	mean=0.22% std=5.64%	Section 3.3.1
Laminar friction factor	Eqn. (3.34)	Uniform	±20%	Own judgment
Forced convection $Nu_{FC,turb}$	Eqn. (3.26)	Normal	mean=0.13% std=5.02%	Section 3.3.2
Forced convection $Nu_{FC,lam}$	Eqn. (3.36)	Uniform	±20%	Own judgment
Natural convection $Nu_{NC,turb}$	Eqn. (3.5)	Uniform	±20%	Own judgment
Natural convection $Nu_{NC,lam}$	Eqn. (3.4)	Uniform	±20%	Own judgment
Lam-Turb Transition $Re_{lim,1}$	2500	Uniform	2000 - 3000	Own judgment
Lam-Turb Transition $Re_{lim,2}$	4000	Uniform	3800 - 5000	Own judgment
Fully Developed Boiling	Eqn. (3.28)	Normal	mean=1.3% std=10.1%	Section 3.3.3

The time evolutions of the PCT, NVGR and CHFR are shown in Figure 6.5. The best-estimate predictions, the 95-95 one-sided tolerance limits, and the maximum or the minimum values, are included in the plots. In addition, a summary is reported in Table 6.2.

None of the safety criteria is exceeded, and sufficiently large margins exist. The peak cladding temperature is largely below 400 °C in all calculations. The estimated tolerance limit is equal to 124.9 °C and the simulations never reach values that are greater than 131.6 °C. The time evolution of the maximum and the upper tolerance limit are similar to the best-estimate case with minor differences of the time for the scram and for the initiation of the safety systems.

The net vapor generation ratio and the critical heat flux ratio in the hot channel are always larger than 1. The beginning of the transient corresponds to the worst conditions, i.e. the reactor is at full power and the core mass flow rate is significantly decreasing. Therefore, the two ratios decrease and reach minimum values at the time of the scram. In terms of 95-95 one-sided tolerance limits, the minimum NVGR is 4.902 and the minimum CHFR is 2.923. The lowest NVRG estimated from all the

calculations however occurs at t = 1316 s (just after the opening of the valves for the natural convection), due to an early occurrence of the reactor scram in the simulation.

Table 6.2: Propagation of uncertainties: summary of the main results.

	BE value	**95%-95% limit**	**Min (or max) value**
Peak cladding temperature [°C]	110.6	124.9	131.6
Minimum NVGR	7.611	4.902	3.868
Minimum CHFR	3.792	2.923	2.733

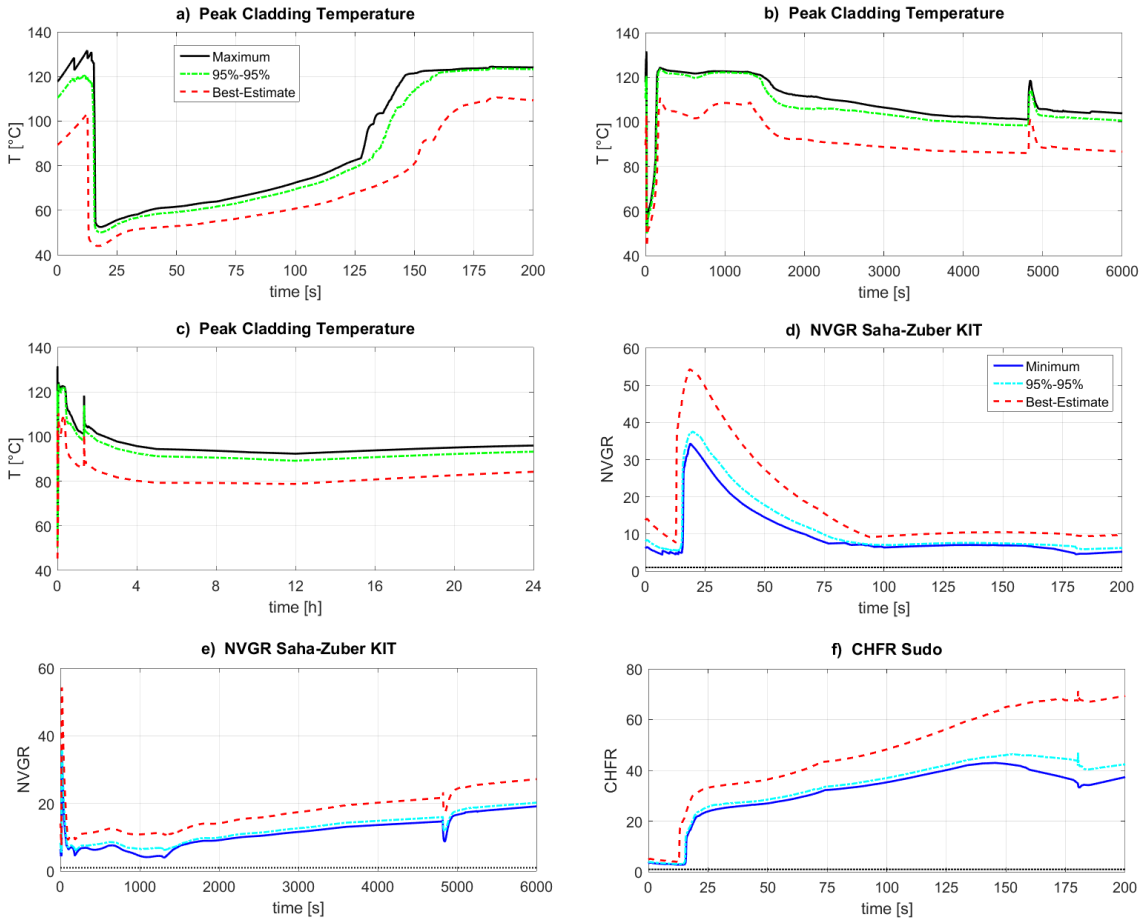

Figure 6.5: Propagation of uncertainties: time evolution of the criteria.

6.5 Sensitivity analysis

The samples generated for the uncertain input parameters and the samples obtained for the peak cladding temperature, the NVGR and the CHFR, are used to compute the standardized regression coefficients, the Pearson correlation coefficients, and the Spearman correlation coefficients. To discriminate whether the correlation coefficients are meaningful or not, a critical value of 0.2 is chosen. This value corresponds to a very low significance level with respect to the size of the sample equal to 336, i.e. about 0.000023 for the case of a two-tailed test [62]. The three sensitivity measures for the three safety parameters are shown in Figure 6.6, 6.7 and 6.8, and they give consistent results.

The peak cladding temperature is impacted by:

- the gap size (its increase determines a decrease in PCT and vice versa);
- the initial core power and the peaking factor (the increase of these parameters leads to an higher PCT);
- the heat transfer coefficient in laminar convection (a better heat transfer coefficient reduces the PCT).

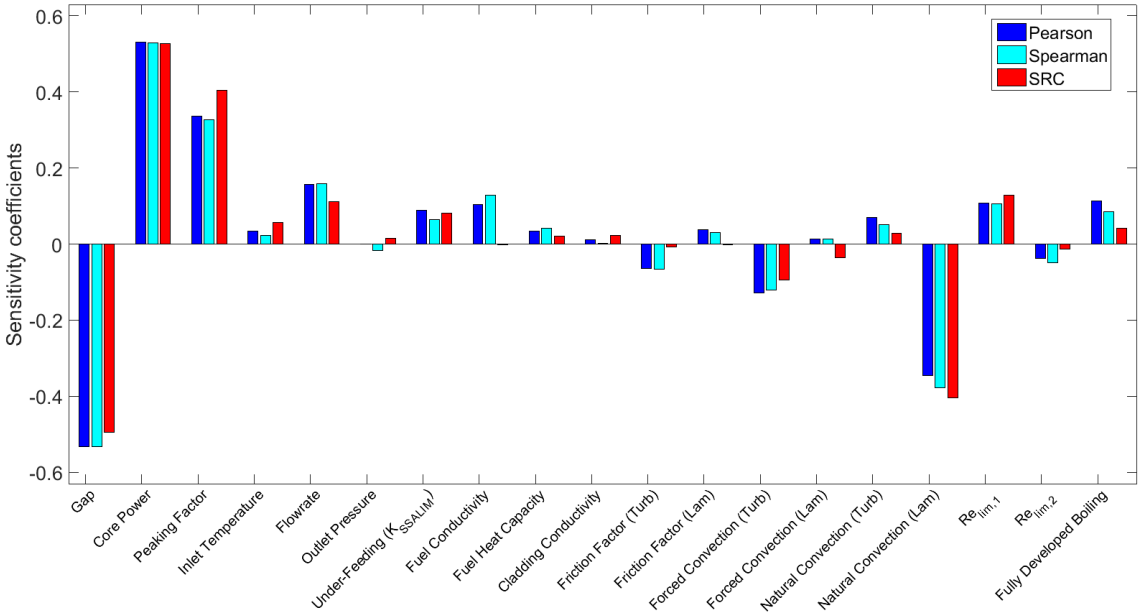

Figure 6.6: Sensitivity analysis for the Peak Cladding Temperature.

The minimum NVGR is mainly influenced by:

- the gap size with a positive correlation (a larger flow area allows a larger mass flow rate);
- the core power and the peaking factor according to a negative correlation;
- a small effect also arises from the total core flow rate at the beginning of the transient.

The minimum CHFR is sensitive to:

- the core power and the peaking factor (smaller values of CHFR are obtained from higher values of these parameters);
- the core mass flow rate (its increase delays the scram initiation, leading to a decrease of the CHFR);
- the gap size with a relatively weak positive correlation.

The other correlation coefficients do not exceed the critical value of 0.2, thus the corresponding input parameters provide a negligible contribution.

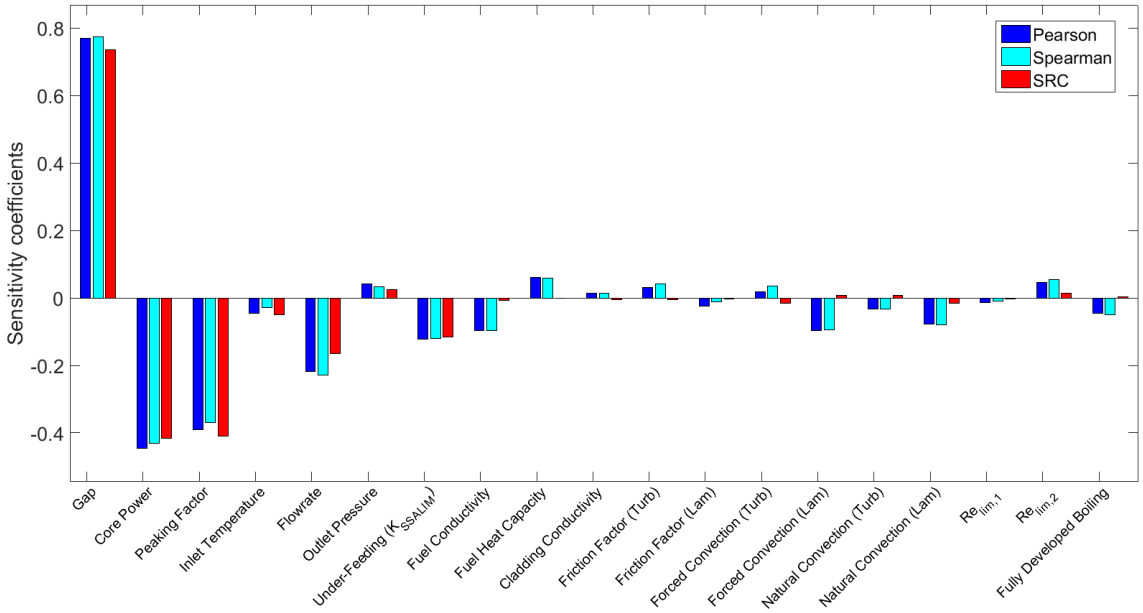

Figure 6.7: Sensitivity analysis for the Net Vapor Generation Ratio.

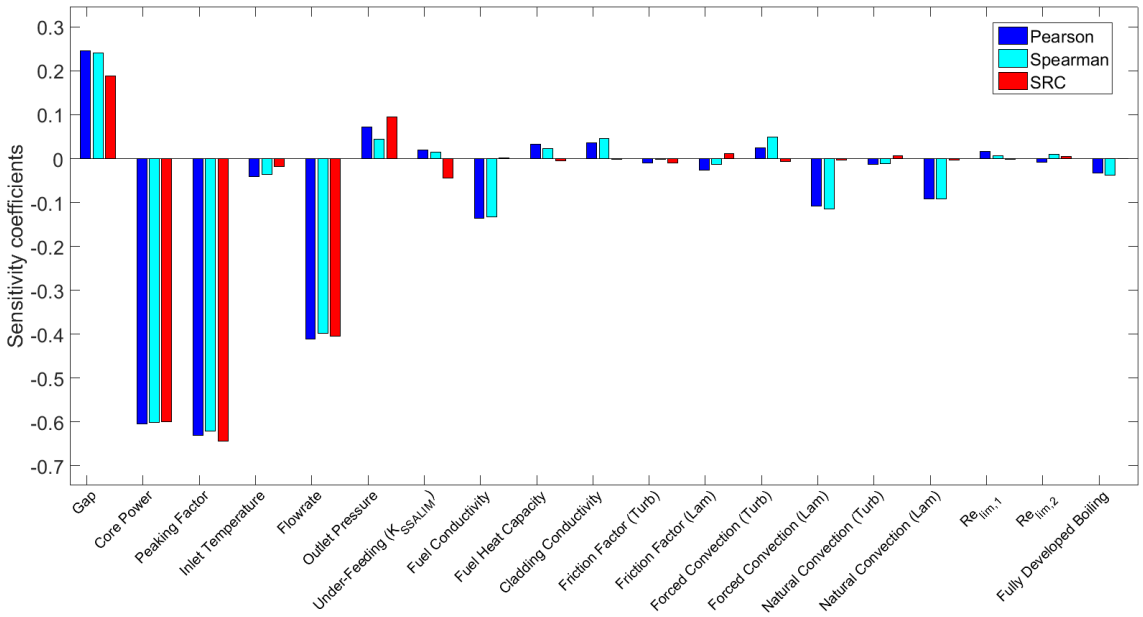

Figure 6.8: Sensitivity analysis for the Critical Heat Flux Ratio.

Chapter 7

Conclusions and recommendation for future work

In this doctoral thesis, thermal-hydraulic correlations, criteria and methods have been investigated with respect to specific aspects of the safety analysis of the Jules Horowitz Reactor, which is a new material testing reactor under construction in France.

7.1 Summary and conclusions

The conclusions may be arranged according to the three main parts of the thesis, and they are related to: the thermal-hydraulic correlations (Paper I, II and Chapter 3); the criteria for the onset of flow instability (Paper III and Chapter 4); the uncertainty and sensitivity analysis for the simulation of a station blackout scenario in the JHR (Paper IV and Chapter 6).

7.1.1 Thermal-hydraulic correlations

The SULTAN-JHR database has been used to assess different types of correlations. The database includes experiments in two narrow rectangular channels, one with gap size of 2.161 mm (SE4) and one with gap size of 1.509 mm (SE3).

7.1.1.1 Single-phase turbulent flow

The single-phase turbulent friction factor for Reynolds numbers between 1.0×10^4 and 3.1×10^5 is under-estimated by the conventional Blasius correlation, therefore a relationship optimized over the SULTAN-JHR tests is applied.

For the single-phase turbulent heat transfer, the SE4 experiments have Reynolds numbers between 1.0×10^4 and 2.69×10^5, while the same kind of experiments in SE3 are between 1.0×10^4 and 1.77×10^5. The main results of the analysis can be summarized as follows:

- Different correlations have been evaluated (Dittus-Boelter, Seider-Tate, etc.) and they under-predict the experimental data, especially at high Reynolds number.

- Such an under-estimation becomes larger for the test section with the smallest gap, suggesting that a reduction of the gap size may enhance the heat transfer in narrow rectangular channels.

- Optimized correlations for each test section have been developed from the best-fitting of the SULTAN-JHR experiments.

7.1.1.2 Fully developed boiling

The SULTAN-JHR experiments used for the fully developed boiling correlations, cover the following conditions: mass flux between 500 and 5364 kg/m^2/s; pressure between 0.23 and 0.9 MPa; steam quality between -0.08 and 0.08; liquid sub-cooling between 0 and 38.5 °C; and heat flux between 0.46 and 4.41 MW/m^2. The outcomes are such that:

- The correlation of Jens-Lottes, Thom, Belhadj, Qiu, and Fabrega, can poorly predict the wall superheat.

- The Gorenflo correlation and a simplified version of the Forster-Greif correlation lead to good results.

- The simplified Forster-Greif correlation combines a good performance with a straightforward implementation.

7.1.1.3 Critical Heat Flux

For the critical heat flux, the SULTAN-JHR experiments were carried out with: pressure between 0.377 and 0.866 MPa; mass flux between 1178 and 6578 kg/m^2/s; inlet sub-cooling between 56.4 and 156.4 °C; outlet steam quality between -0.008 and 0.178. The main findings are:

- The standard Groeneveld look-up tables significantly overestimate the CHF and they give non-conservative results.

- Doerffer's formula over-estimates the experiments in SE3 and under-estimate the ones in SE4.

- The Sudo correlation performs well for SE4 and over-predict the SE3 experiments.

7.1.1.4 Proposed correlations for the JHR model

From the above results, modifications of the CATHARE code have been proposed to improve the thermal-hydraulic model of the JHR. The recommendations are:

- The relationship Eqn. (3.21) derived from the SULTAN-JHR tests, can estimate the single-phase turbulent friction in an adequate manner.

- The relationship Eqn. (3.26), which is optimized over the SULTAN-JHR experiments in SE4, can be used for the single-phase turbulent heat transfer.

- The correlation of Forster-Greif can be applied to determine the superheat in the case of fully developed boiling.
- The Sudo correlation can be a reasonable choice for estimating the CHF.
- In addition, a simplified model for the laminar-turbulent transition has been included in CATHARE, so that possible over-estimation of the heat transfer can be avoided at low Reynolds number.

7.1.2 Onset of Flow Instability

Several criteria for the onset of flow instability are assessed against relevant experiments in vertical heated rectangular channels with gap sizes between 1.27 and 3.6 mm. The data come from the SULTAN-JHR database and from the literature, and cover the following range of conditions: mass fluxes between 740 and 20325 kg/m^2/s; pressures between 0.12 and 1.73 MPa; heat fluxes between 0.4 and 14.9 MW/m^2; Peclet numbers between 15889 and 358460.

7.1.2.1 Main results of the assessment

The findings can be summarized as:

- The criteria based on ONB can lead to very conservative predictions, as to be expected since the formation of bubbles at the heated walls is a prerequisite for OFI.
- The FDB-based criteria estimate the OFI condition in most of the tests, although they could not capture OFI in some of the channels with small gap size.
- The NVG criteria can predict the majority of the experiments, and the results are generally conservative within a relatively narrow spread. However, the Saha-Zuber correlation fails at low Peclet numbers (lower than 70000), suggesting a different value of Peclet for the transition between thermally and hydro-dynamically driven bubble detachment.
- The NVG criterion based on the Saha-Zuber KIT correlation can identify OFI in all the experiments.
- 'Global' criteria such as the Whittle-Forgan and Stelling FIRs give results close to the ideal value, with relatively small standard deviations. Nevertheless, they cannot predict some experiments in channels with small gaps or at high Peclet numbers.
- A criterion based on the combination between the Stelling FIR and the Saha-Zuber KIT correlation was optimized over the available experimental data.
- An axially non-uniform heat flux profile may affect the results. In particular, the global criteria developed under uniform heat flux conditions, may be conservatively applied when the heat flux at the end of the heated test section is smaller than the average one and vice versa.

7.1.2.2 Suggestions for the JHR analysis

For the analysis of the onset of flow instability in the case of JHR, the criterion based on the Saha-Zuber KIT correlation is a viable option. In fact it has been shown to lead to conservative and good results, and it can be extended straightforward to the CATHARE code where the necessary correlation is already implemented.

7.1.3 Simulation of a station blackout scenario in the JHR

The modified version of the CATHARE code according to the outcomes of Chapter 3, has been combined with a best-estimate plus uncertainty approach for the analysis of the JHR. Since more realistic models have been included and the conservatism has been reduced to some extent, it is important to evaluate the impact of the input and modeling uncertainties on the calculation of the safety margins.

As a test case, a postulated Station Blackout scenario in the JHR has been simulated. Input and modeling uncertainties have been quantified and propagated to the code results using the GRS methodology. The focus of the analysis has been on three safety parameters, namely: the peak cladding temperature, the net vapor generation ratio, and the critical heat flux ratio. The estimation of the 95-95 one-sided tolerance limits relies on 336 calculations and it has been shown that:

- The peak cladding temperature reaches a maximum value of 124.9 °C, which is below the acceptance limit equal to 400 °C.
- The minimum value of NVGR is 4.902, so that no onset of flow instability occurs during the transient.
- The minimum value of CHFR is 2.923, so no critical heat flux is reached.

From the sensitivity analysis, it has been found that:

- The three safety parameters are affected by the possible uncertainties in the gap size of the hot channel, in the core power and in the peaking factor.
- The mass flow rate plays a role in the estimation of the NVGR and the CHFR.
- When the natural convection comes into play, then the accuracy of the relative model may have a significant impact on the peak cladding temperature.

7.2 Recommendations for future work

This research has identified some open issues that would require further investigations. In particular, the following recommendations for future work can be made:

- The gap size and the width-to-gap ratio of a narrow channel play a crucial role in the heat transfer. However, the available experimental data do not allow a full understanding of the phenomenon. In order to develop models including the dependence of the geometrical parameters, a systematic campaign of experiments using different test sections can provide valuable data.

- In system codes, reliable simulations of the two-phase flow and of the boiling heat transfer are essential. Thus, experiments in narrow channels with void fraction measurements would be useful for the validation work.
- During the progression of an accident, the reactor can operate at low coolant velocities, and consequently at low Reynolds numbers. There is a scarcity of experiments for these cases and additional data are needed for a more accurate modeling of the laminar-turbulent transition.
- The low velocities of the coolant correspond also to low Peclet numbers in the reactor. More experiments are therefore required for a better understanding and modeling of the onset of flow instability under these conditions.

Acknowledgments

I would like to thank all the people who contributed to the completion of my doctoral studies.

First of all, I want to express my sincere gratitude to my main supervisors Dr. Brigitte Noel and Assoc. Prof. Paolo Vinai for their continuous scientific and moral support, guidance and supervision. The fruitful and pleasant discussions, the comments and the suggestions were of great help for overcoming the encountered difficulties and to improve the quality of the work. I have really appreciated the respectful and encouraging attitude towards me, the good company and the nice working environment.

I am also very grateful to Prof. Christophe Demazière for his helpful comments and feedbacks on the research work and to Prof. Imre Pazsit for being my examiner.

Many thanks go to my colleagues both at Chalmers and at CEA-Grenoble for creating a pleasant working environment. Special gratitude goes to Dr. Marc Parent for his support with CATHARE and to Dr. Didier Dumont for his help.

I would also like to acknowledge the JHR team for their cooperation and support to the project. Special thanks goes to Dr. Serge Bourdon for providing data and useful suggestions, to Dr. Gilles Bignan and Dr. Xavier Bravo for their help.

Thanks to Dr. Dominique Bestion, Prof. Kostadin Ivanov, Assoc. Prof. Annalisa Manera, Dr. Victor Sanchez for accepting to be in the grading committee.

The financial support of the Swedish Research Council (Vetenskapsrådet) is gratefully acknowledged and appreciated (contract number: B0774701).

Last but not least, I would like to express my gratitude to my family which has been supporting and encouraging me during my entire life.

Thank you very much! Tack så mycket! Merci beaucoup! Grazie mille!

Bibliography

[1] D. Iracane. The JHR, a new material testing reactor in Europe. *Nuclear Engineering and Technology*, 38:437–442, 2006.

[2] Nuclear Physics European Collaboration Committee (NuPECC). Nuclear physics for medicine. Technical report, Strasbourg, France, 2014.

[3] F. Barre and M. Bernard. The CATHARE code strategy and assessment. *Nuclear Engineering and Design*, 124:257–284, 1990.

[4] J. G. Collier and J. R. Thome. *Convective boiling and condensation*. Clarendon Press, Oxford, UK, 1994.

[5] J.A.Boure, A.E. Bergles, and L.S. Tong. Review of two-phase flow instability. *Nuclear Engineering and Design*, 25:165–192, 1973.

[6] M. Ledinegg. Instability of flow during natural and forced circulation. *Die Wärme*, 61:891–898, 1938.

[7] R. H. Whittle and R. Forgan. A correlation for the minima in the pressure drop versus flow-rate curves for sub-cooled water flowing in narrow heated channels. *Nuclear Engineering and Design*, 6:89–99, 1967.

[8] M. Siman-Tov, D. K. Felde, J. L. McDuffee, and G. L. Yoder. Experimental study of static flow instability in subcooled flow boiling in parallel channels. In *Proceedings of the 4th ASME/JSME Thermal Engineers Joint Conference*, Maui, Hawaii, 1995.

[9] I. Babelli and M. Ishii. Flow excursion instability in downward flow systems. Part I. Single-phase instability. *Nuclear Engineering and Design*, 206:91–96, 2001.

[10] G. Geffraye, O. Antoni, M. Farvacque, D. Kadri, G. Lavialle, B. Rameau, and A. Ruby. CATHARE 2 V2.5_2: A single version for various applications. *Nuclear Engineering and Design*, 241:4456–4463, 2011.

[11] G. Lavialle. General description of the CATHARE 2 V25_2mod8.1 system code. Technical report, CEA, 2012.

[12] H. Blasius. Das ähnlichkeitsgesetz bei reibungsvorgängen in flüssigkeiten. *Forschg. Arb. Ing.-Wes.*, 131, 1913. Obtained from secondary reference: [13].

[13] S. Kakaç, R. K. Shah, and W. Aung, editors. *Handbook of single-phase convective heat transfer*. John Wiley & Sons, 1987.

[14] F. W. Dittus and L. M. K. Boelter. Heat transfer in automobile radiators of the tubular type. *University of California Publications in Engineering*, 2:3–22, 1930.

[15] R. W. Bowring. Physical model, based on bubble detachment and calculation of voidage in the subcooled region of a heated channel. Technical Report HPR10, Halden, Norway, 1962. Obtained from secondary reference: [4].

[16] J. R. S. Thom, W. M. Walker, T. A. Fallon, and G. F. S. Reising. Boiling in subcooled water during flow up heated tubes or annuli. In *Proceedings of Symposium on Boiling Heat Transfer in Steam Generation Units and Heat Exchangers*, Manchester, UK, 1965. Obtained from secondary reference: [4].

[17] A. Ghione. Improvement of the nuclear safety code CATHARE based on thermal-hydraulic experiments for the Jules Horowitz Reactor. Licentiate thesis: CTH-NT-306, Chalmers University of Technology, Gothenburg, Sweden, 2015.

[18] P. Saha and N. Zuber. Point of Net Vapor Generation and vapor void fraction in subcooled boiling. In *Proceedings of the 5th International Heat Transfer Conference*, volume 4, pages 175–179, Tokyo, Japan, 1974.

[19] V. Kalitvianski. Qualification of CATHARE 2 V1.5 Rev. 6 on subcooled boiling experiments (KIT tests). Technical report, CEA, Grenoble, France, 2000.

[20] L. Sabotinov. *Experimental investigation of the void fraction at subcooled boiling for different heat flux profiles along the channel*. PhD thesis, Moscow Power Engineering Institute, Moscow, Russia, 1974.

[21] D. C. Groeneveld, S. C. Cheng, and T. Doan. 1986 AECL-UO critical heat flux lookup table. *Heat Transfer Engineering*, 7:46–62, 1986.

[22] M. Siman-Tov, D. K. Felde, G. Farquharson, J. L. McDuffee, M. T. McFee, A. E. Ruggles, M. W. Wendel, and G. L. Yoder. FY 1995 Progress report on the ANS Thermal-Hydraulic Test Loop operation and results. Technical Report ORNL/TM-12972, Oak Ridge National Laboratory, Tennessee, USA, 1997.

[23] M. W. Croft. Advanced test reactor. Burnout heat transfer tests. Technical Report USAEC IDO-24465, Babcock & Wilcox, Lynchburg, Virginia, USA, 1964.

[24] W. R. Gambill and R.D. Bundy. Heat-transfer studies of water flow in thin rectangular channels. Part I - Heat Transfer, Burnout and Friction for water in turbulent forced convection. *Nuclear Science and Engineering*, 18:69–79, 1964.

[25] J. Costa. Mesure du coefficient de frottement en écoulement turbulent simple phase liquide avec transfert de chaleur dans un canal rectangulaire. Technical Report N-1142, CEA, Grenoble, France, 1969.

[26] S. Levy, R. A. Fuller, and R. O. Niemi. Heat transfer to water in thin rectangular channels. *Journal of Heat Transfer*, pages 129–143, 1959.

[27] J. Ma, L. Li, Y. Huang, and X. Liu. Experimental studies on single-phase flow and heat transfer in a narrow rectangular channel. *Nuclear Engineering and Design*, 241:2865–2873, 2011.

[28] Z. H. Liang, Y. Wen, C. Gao, W. X. Tian, Y. W. Wu, G. H. Su, and S. Z. Qiu. Experimental investigation on flow and heat transfer characteristics of single-phase flow with simulated neutronic feedback in narrow rectangular channel. *Nuclear Engineering and Design*, 248:82–92, 2012.

[29] E. N. Sieder and G. E. Tate. Heat transfer and pressure drop of liquids in tubes. In *Proceedings of the Heat Transfer Symposium*, pages 1429–1435, Division of Industrial and Engineering Chemistry, Yale University, USA, 1936.

[30] K. Engelberg-Forster and R. Greif. Heat transfer to a boiling liquid; mechanism and correlations. *Journal of Heat Transfer*, 81:43–53, 1959.

[31] A. P. Olson and M. Kalimullah. A user's guide to the PLTEMP/ANL code (version 4.2). Technical Report ANL/RERTR/TM-11-22 Ver. 4.2, Argonne national laboratory, Illinois, USA, 2015.

[32] R. Ricque and R. Siboul. Etude expérimentale de l'échange thermique à flux élevé avec l'eau en convection forcée à grande vitesse dans des tubes de petit diamètre, avec et sans ébullition. *International Journal of Heat and Mass Transfer*, 15:579–592, 1972.

[33] R. K. Shah and A. L. London. Laminar flow forced convection in ducts. In *Advances in Heat Transfer*. Academic Press, New York, 1978. Obtained from secondary references: [13] and [36].

[34] C. Wang, P. Gao, S. Tan, Z. Wang, and C. Xu. Experimental study of friction and heat transfer characteristics in narrow rectangular channel. *Nuclear Engineering and Design*, 250:646–655, 2012.

[35] S. M. Marco and L. S. Han. A note on limiting laminar Nusselt number in ducts with constant temperature gradient by analogy to thin-plate theory. *Transactions of the ASME*, 77:625–630, 1955. Obtained from secondary reference: [13].

[36] Y. A. Çengel. *Heat Transfer: a practical approach*. Mcgraw-Hill, 2nd edition, 2002.

[37] M. Courtaud, K. Schleisiek, G. Coulon, and F. Mazzili. Compte rendu d'essais. Pertes de charge et redistribution de débit sur des canaux rectangulaires de 1.8 mm d'entrefer (type R.H.F.). Technical Report TT/67-7/B/MC-KS-GC-FM, CEA, Grenoble, France, 1967.

[38] M. Courtaud, G. Coulon, and F. Mazzili. Compte rendu d'essais. Boucle CASIMIR: Traces de courbes en S. 1ère partie: Eau dégazée. Technical Report TT/66-2/B/MC-GC-FM, CEA, Grenoble, France, 1966.

[39] M. Courtaud, G. Coulon, and F. Mazzili. Compte rendu d'essais. Boucle CASIMIR: Traces de courbes en S (canal de 900 mm). Essais de dépressurisation. Technical Report TT/66-7/B/MC-GC-FM, CEA, Grenoble, France, 1966.

[40] P. Vernier. Compte rendu d'essais. OSIRIS - Etude de sûreté. Détermination expérimentale des courbes en S et des conditions de redistribution de débit. Technical Report TT/65-19-B/PV, CEA, Grenoble, France, 1965.

[41] K. Schleisiek and J. C. Dumaine. Compte rendu d'essais. Essais préliminaires pour RHF: Détermination expérimentale des conditions de redistribution de débit a des pressions comprises entre 4 et 5 kg/cm^2 abs pour un canal rectangulaire de 2 mm d'épaisseur et de 60 cm de longeur. Technical Report TT/66-10-B/KS-JCO, CEA, Grenoble, France, 1966.

[42] M. Courtaud, G. Coulon, and F. Mazzili. Compte rendu d'essais. Boucle CASIMIR: Traces de courbes en S sur des canaux a flux non uniforme. Technical Report TT/66-14/B/MC-KS-GC-FM, CEA, Grenoble, France, 1966.

[43] M. Courtaud, G. Coulon, and F. Mazzili. Compte rendu d'essais. Boucle CASIMIR: Traces de courbes en S. 2ème partie: Eau gazée. Technical Report TT/66-5/B/MC-GC-FM, CEA, Grenoble, France, 1966.

[44] P. Raymond, B. Spindler, and R. Lenam. Pressurized water reactor thermal-hydraulic core analysis with the FLICA computer code. *Nuclear Engineering and Design*, 124:299–313, 1990.

[45] R. Pegonen, S. Bourdon, C. Gonnier, and H. Anglart. A review of the current thermal-hydraulic modeling of the Jules Horowitz Reactor: A loss of flow accident analysis. *Nuclear Engineering and Design*, 280:294–304, 2014.

[46] A. E. Bergles and W. M. Rohsenow. The determination of forced-convection surface-boiling heat transfer. *Journal of Heat Transfer*, 86:365–372, 1964.

[47] R. Stelling, T. Dougherty E. V. McAssey Jr., and B. W. Yang. The onset of flow instability for downward flow in vertical channels. *Journal of Heat Transfer*, 118:709–714, 1996.

[48] A. P. Olson. Analysis of flow excursion experiments relevant to research reactors: revisited. In *Proceedings of the International Meeting on Reduced Enrichment for Research and Test Reactors (RERTR)*, Cape Town, South Africa, 2006.

[49] International Atomic Energy Agency. Research reactor core conversion guidebook. Technical Report IAEA-TECDOC-643, Vienna, Austria, 1992.

[50] J. Lee, H. Chae, and S. H. Chang. Flow instability during subcooled boiling for a downward flow at low pressure in a vertical narrow rectangular channel. *International Journal of Heat and Mass Transfer*, 67:1170–1180, 2013.

[51] International Atomic Energy Agency. Best estimate safety analysis for nuclear power plants: Uncertainty evaluation. Technical Report IAEA Safety Reports Series N. 52, 2008.

[52] U.S. Nuclear Regulatory Commission. Acceptance criteria for emergency core cooling systems for light-water nuclear power reactors. Code of Federal Regulations: 10 CFR 50.46, 2007.

[53] A. Petruzzi and F. DAuria. Evaluation of uncertainties in system thermal-hydraulic calculations and key applications by the CIAU method. *International Journal of Nuclear Energy Science and Technology*, 4:111–131, 2008.

[54] B.E. Boyack, I. Catton, R. B. Duffey, P. Griffith, K. R. Katsma, G. S. Lellouche, S. Levy, U. S. Rohatgi, G. E. Wilson, W. Wulff, and N. Zuber. Quantifying reactor safety magins. part 1: An overview of the Code Scaling, Applicability and Uncertainty evaluation method. *Nuclear Engineering and Design*, 119:1–15, 1990.

[55] H. Glaeser. GRS method for uncertainty and sensitivity evaluation of code results and applications. *Science and Technology of Nuclear Installations*, 2008:1–7, 2008.

[56] A.D. Kiureghian and O. Ditlevsen. Aleatory or epistemic? Does it matter? *Structural Safety*, 31:105–112, 2008.

[57] S. S. Wilks. Determination of sample sizes for setting tolerance limits. *The Annals of Mathematical Statistics*, 12:91–96, 1941.

[58] P. N. Somerville. Tables for obtaining non-parametric tolerance limits. *The Annals of Mathematical Statistics*, 29:599–601, 1958.

[59] P. Vinai, R. Macian-Juan, and R. Chawla. A statistical methodology for quantification of uncertainty in best estimate code physical models. *Annals of Nuclear Energy*, 34:628–640, 2007.

[60] H. Glaeser, P. Bazin, J. Baccou, E. Chojnacki, and S. Destercke. BEMUSE phase VI report: Status report of the area, classification of the methods, conclusions and recommendations. Technical Report NEA/CSNI/R(2011)4, OECD, 2011.

[61] J.C. Helton, J. D. Johnson, C. J. Sallaberry, and C. B. Storlie. Survey of sampling-based methods for uncertainty and sensitivity analysis. *Reliability Engineering and System Safety*, 91:1175–1209, 2006.

[62] R. A. Fisher. *Statistical methods for research workers.* Oliver and Boyd, 1958.

[63] F. Gaudier. URANIE: The CEA/DEN Uncertainty and Sensitivity platform. *Procedia - Social and Behavioral Science: Special issue on the Sixth International Conference on Sensitivity Analysis of Model Output*, 2:7660–7661, 2010.

[64] CERN. ROOT data analysis framework. `https://root.cern.ch/`. Accessed: 2016-09-14.

[65] R. Pegonen, S. Bourdon, C. Gonnier, and H. Anglart. Hot fuel element thermal-hydraulics in the Jules Horowitz Reactor. *Nuclear Engineering and Design*, 300:149–160, 2016.